

Review of Aeronautical Fatigue Investigations in Switzerland

May 2011 – March 2013

ZAV Document 2013

**Dr. M. Guillaume
Zurich University of Applied Sciences
ZHAW / School of Engineering
Centre for Aviation**

SUMMARY

The Swiss review summarizes fatigue work in Switzerland. It includes main contributions from the Zurich University of Applied Sciences (ZHAW), RUAG Switzerland Ltd. (RUAG Aviation), CFS Engineering. This document forms a chapter of the ICAF conference minutes published by the conference host nation. The format of the review reflects ICAF requirements.

Prepared for the presentation at the 33th ICAF Conference
Jerusalem, 03 and 04 June 2013

SUMMARY	1
4.1 Introduction	4
4.2 New Reference Flaws for Ultrasonic Testing of Carbon Composites structures	5
4.3 Investigation on the effect of hydraulic fluid contamination in adhesive joints in composites repairs	6
4.4 CERFAC (Cost Effective Reinforcement of Fastener Areas in Composites).....	8
4.5 Assessment and Fatigue Lifetime of Repaired Nickel Based Superalloys	10
4.6 Swiss / Finnish Computational Fluid Dynamics Simulation on the F/A-18	11
Model Development.....	11
Swiss Approach:.....	11
Finish Approach:.....	13
Results.....	15
Load Cases:	16
Sensitivity Analysis of CFD Calculations.....	18
Structural Component Loads.....	19
Conclusion & Outlook.....	22
4.7 Development of new Grid for F/A-18 CFD Loads Calculations	23
Introduction.....	23
Strategy Grid Generation.....	23
Conclusion.....	24
Chimera solid Components	24
Lessons Learned	25
4.8 Investigation of Ex-Military Planes under civil Usage	26
Introduction.....	26
Pilatus P3 Test	27
Venom Test	27
4.8 F/A-18 Structural Activities Master Plan	29
Introduction.....	29
Collection of Damage Information	29
Structural Activities Master Plan.....	30
Analysis of the Damages.....	31
Way ahead.....	32
4.9 Quantitative Fractographic Analysis of Swiss F/A-18 D Full Scale Fatigue Test Locations	33

5.0	Evaluation of Marker Loads for Variable Amplitude Spectrum Coupon Test	36
	Introduction	36
	Approach	36
	Testing and Results	37
	Mini Falstaff Baseline	37
	Reordering	38
	Underloads/Overloads	38
	Constant Amplitude with two different R-ratios	38
5.1	Effect of Corrosion on Structural Integrity of an Aluminum Wing Lower Skin of a Fighter Aircraft.....	42
5.2	Fretting Fatigue Testing and Repair Qualification of a Wing to Fuselage Trunnion ...	44

4.1 Introduction

The present review gives a brief summary of the work performed in Switzerland in the field of aeronautical fatigue, during the period from May 2011 till March 2013. The various contributions to this review come from the following sources:

- Zurich University of Applied Sciences (ZHAW); School of Engineering, Institute of Material Processing & Centre for Aviation
- RUAG Switzerland Ltd., RUAG Aviation; Structural Engineering, Aerodynamic Engineering
- CFS Engineering, Lausanne

All the interesting contributions are gratefully acknowledged, especially the effort of Prof. Dr. Arnd Jung (ZHAW), Gregor Peikert (ZHAW), and Andreas Uebersax (RUAG Aviation).

4.2 New Reference Flaws for Ultrasonic Testing of Carbon Composites structures

G. Peikert / ZHAW

Ultrasonic Testing of Carbon Composite structures requires reference panels with known defects. Those defects are usually manufactured with release film inserts. However the inspector never knows whether he is detecting a non-bond (delamination) or the presence of a release film.

In a study a new method for manufacturing of real disbonds was developed.

The work includes the manufacturing and non-destructive testing of artificial flaws in CFRP (carbon fibre reinforced plastics) structures like the main landing gear door of the F/A 18 aircraft.

Several test items were developed as reference panels for non-destructive UT and thermography testing. For this purpose, square flaws with a lateral length of 5 mm, 10 mm and 20 mm are inserted in monolithic laminates, in the adhesive layer between two laminates as well as in the adhesive layer between a laminate and an aluminum core. The flaws consist either of permanent inserts made out of different materials like polymer foils, glass fiber fabric and elastomers. The delaminations and disbonds are formed by removing the delamination inserts after the curing process. Using microsections, the thickness of a delamination of just 100 μm was successfully proven.

Three test items with artificial flaws are inspected with phased-array ultrasonics and lock-in thermography. The thermography inspections detect inserts and delaminations from a width of 10 mm. The ultrasonic inspection detects all the inserted flaws. Additionally, this inspection allows to conclude about the reflection power and reflection depth of a structure or flaw. This newly gained knowledge will be integrated in the proposal for a test article of an F/A 18 main landing gear door.

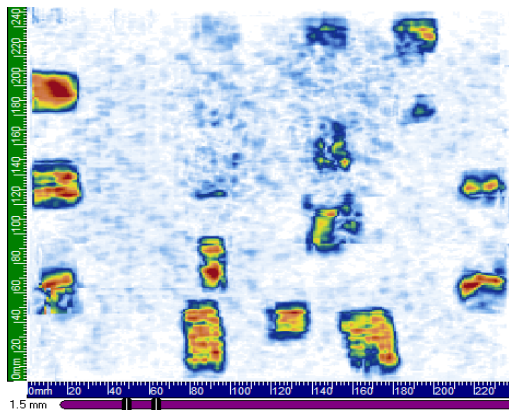


Fig. 1

Phased Array scan of reference panel with different flaw materials



Fig. 2

Microsection of artificially manufactured delamination in Carbon Composite laminate

4.3 Investigation on the effect of hydraulic fluid contamination in adhesive joints in composites repairs

G. Peikert / ZHAW

In collaboration between RUAG Aviation, the US Navy Materials Engineering Laboratory and ZHAW an anomalous behavior of the adhesive used for the repair of composite materials was observed and investigated. The bond strength increases in the presence of a hydraulic fluid contamination.

Laboratory tests were performed to confirm one or more of the following assumptions:

1. The hydraulic fluid acts as a plasticizer
2. The hydraulic fluid activates the surface of the composite materials
3. The hydraulic fluid reacts with the adhesive
4. The hydraulic fluid acts as a solvent

Through mechanical tests such as tensile and shear test, rheological tests such as plate-plate rheometer and DMTA, the DSC analysis and the IR-spectroscopy, it can be concluded that the hydraulic fluid acts as a plasticizer according to the first assumption.

The maximum percentage of hydraulic fluid contained in the adhesive that shows this behavior was fixed to 1%. At this rate the viscosity of the contaminated adhesive is less than the pure sample, while the increase in the Youngs Modulus is approximately 200 MPa (25 psi) (Fig. 3).

The REM microscopy images have confirmed the plasticizer effect of the fluid, as fractures occur with a ductile character. At higher concentrations the performance of the adhesive begins to degrade, due to an aggregation of alumina oxide and fumed silica particles from the adhesives (Fig. 4).

The hydraulic fluid is completely inert in respect of the adhesive (Fig. 5), while the prolonged

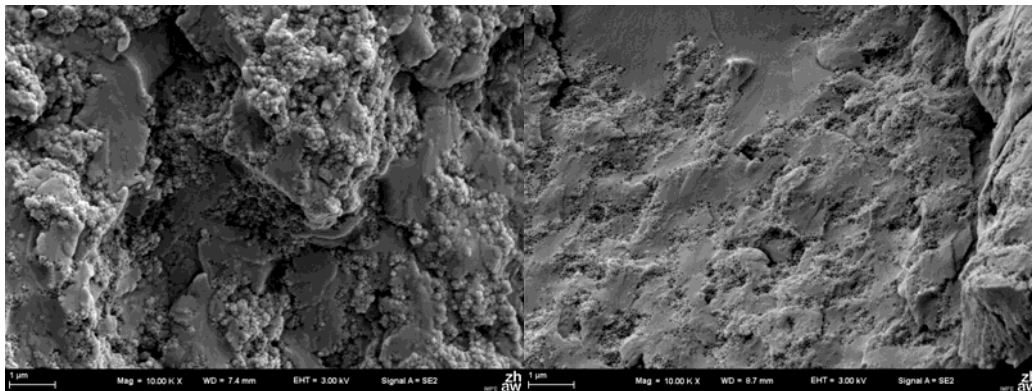


Fig. 3 Tensile modulus of uncontaminated (0%) and contaminated samples.

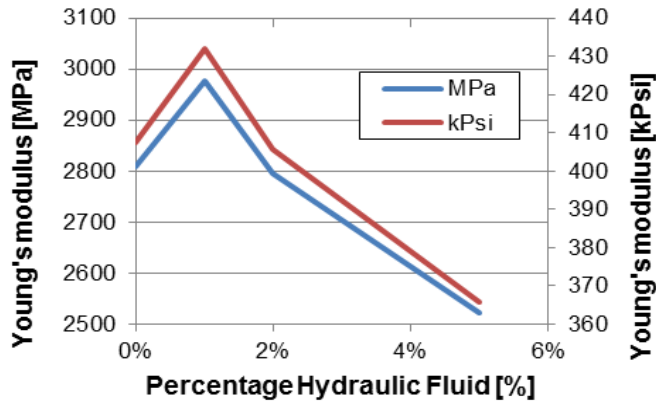


Fig. 4 Agglomeration of pure adhesive and 5% contaminated adhesive.

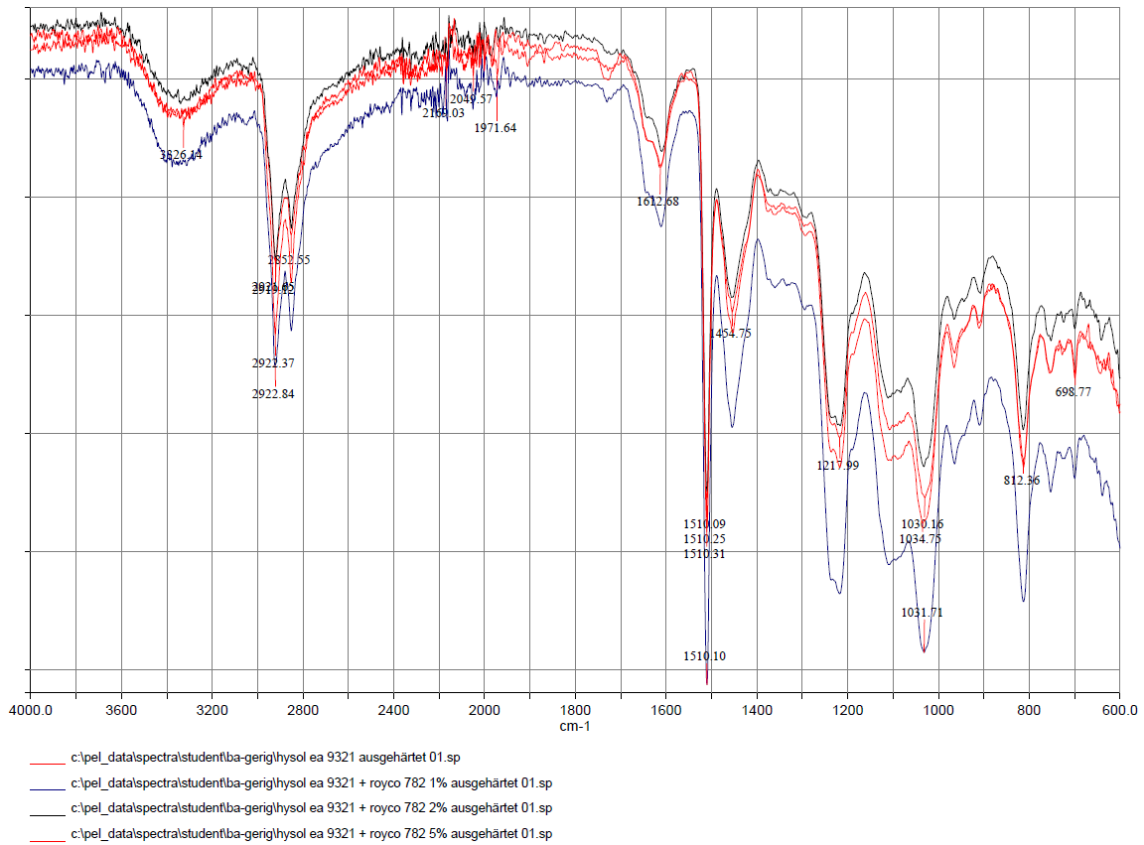


Fig. 5 IR-Spectra of pure adhesive and 1%, 2% and 5% contaminated adhesive. The differences between the spectra are minimal, indicating the absence of any kind of reaction and new bonds between fluid and resin.

4.4 CERFAC (Cost Effective Reinforcement of Fastener Areas in Composites)

Fatigue behavior of patch reinforcement in CFRP panels

G. Peikert / ZHAW

In context with the project CERFAC, the laboratory of composite materials at the Zurich University of Applied Science (ZHAW) developed a new reinforcement solution to increase the bearing strength in CFRP panels.

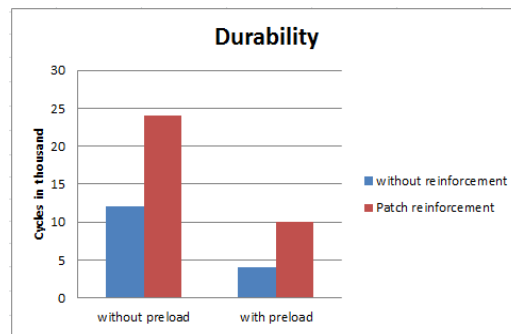
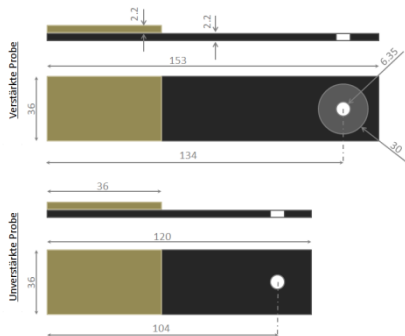


Fig. 6 Specimen with and without patch reinforcement **Fig. 7** Durability of the different samples

The static tests showed an increase of 10% in bearing strength. However, there is no awareness of fatigue behavior. Dynamic tests were performed with 4 different specimens (Fig. 6).

- Sample with patch reinforcement with 2% hole elongation
- Sample with patch reinforcement without hole elongation
- Sample without patch reinforcement with 2% hole elongation
- Sample without patch reinforcement without hole elongation

All the samples were tested with a tensile – tensile load at a frequency of 10 Hz. At higher frequencies vibrations occurred. The tests ended at the hole elongation of 6.93 mm (10%) or 12,000 cycles. To measure the hole elongation every 1000 cycles the samples were disassembled and measured with a slide gauge.

The results show that there is an increase in durability with patch reinforcement. In both cases, whether a preload was applied or not, the patch reinforcement doubled the durability of the bolting (Fig. 7).



Fig. 8 Failure modes of the hole. a) No elongation visible. b) The hole starts to elongate. First delamination of fibers c) The delaminated fibers form a burr d) Bearing failure: permissible strain exceeded e) Rear side of picture d

The failure modes of the samples with and without the patch reinforcement look similar. In Fig. 8 are all the typical failure modes shown at different moments. However, the pilot batch was very small and further tests need to be done.

4.5 Assessment and Fatigue Lifetime of Repaired Nickel Based Superalloys

A. Jung / ZHAW

Nickel based super alloys are widely used in aircraft gas turbine engines as they exhibit excellent high temperature properties and strength due to precipitation hardening by the Ni_3Al γ' phase. Extending engine life and reducing costs associated with component replacement, weld repair of aircraft gas turbine parts has become increasingly prevalent. However, γ' precipitation strengthened alloys have a susceptibility to heat affected zone cracking during welding and during post-weld heat treatment. Modern welding techniques like laser and electron beam welding in connection with appropriate heat treatments are used to recondition ex-service parts.

The Institute of Materials and Process Engineering (IMPE) cooperates with aircraft engine OEM and repair shops for full qualification of repair processes. This includes mechanical and microstructural qualification of the nickel based superalloys. In order to assess the cyclic lifetime of repaired components, strain-controlled low cycle fatigue (LCF) test are performed at the relevant operating temperatures up to 1100°C (Fig. 9). The LCF cycle types are defined according to the real aircraft loading condition enabling lifetime predictions of the repaired components. In order to specify the various steps of the repair process like welding and heat treatments, microstructural assessments of the materials conditions are done (Fig. 10). Combining cyclic lifetimes and microstructural assessments ensures a reliable and reproducible repair of aircraft engine parts.

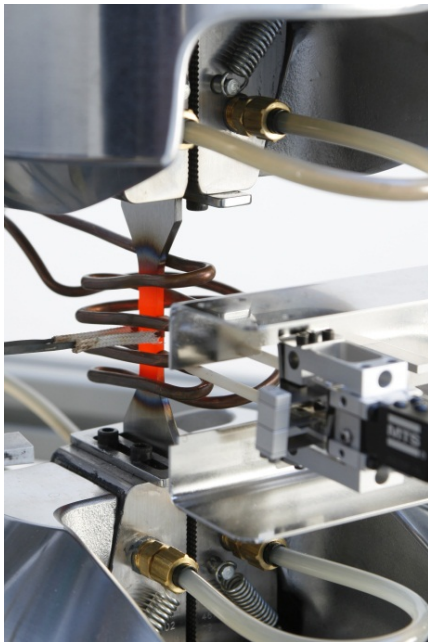


Fig. 9 LCF test on welded IN718 at 650°C

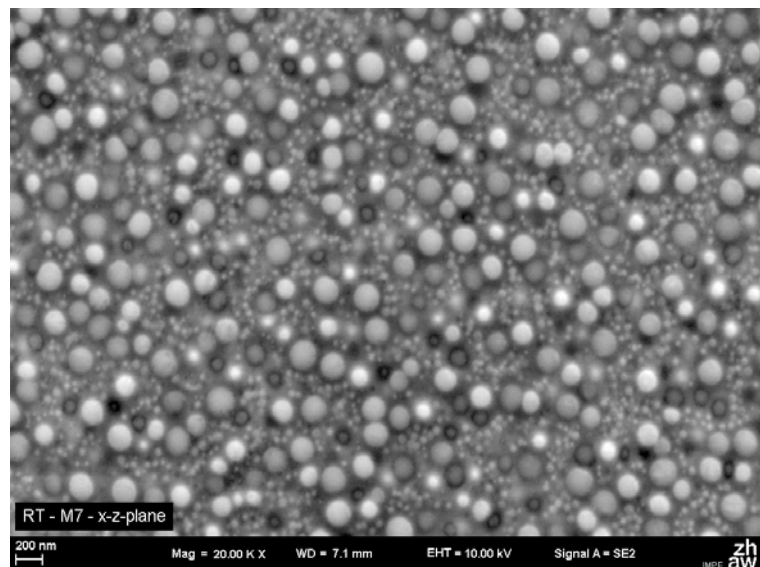


Fig. 10 γ' Distribution of Waspaloy after full heat treatment (SEM)

4.6 Swiss / Finnish Computational Fluid Dynamics Simulation on the F/A-18

M. Guillaume / ZHAW, P. Stephani, A. Gehri / RUAG Aviation, J. Vos / CFSE, T. Siikonen, E. Salminen / FINFLO

The Swiss-Finnish collaboration is very unique and provides a great opportunity to improve the complex CFD calculations on the F/A-18. Both countries will profit from this effort which is much more than just research in the field of advanced CFD calculations. The advantage provides a considerable improvement in mesh grid strategies and in numerical simulation for accurate maneuver loads prediction.

Model Development

Both solvers, NSMB for Switzerland [1, 2] and FINFLO [2, 3] from Finland, are Navier-Stokes codes based on the cell-centered Finite Volume method using multi block structured grids. In this study only symmetrical load conditions are considered therefore half models were used for CFD calculations. The Swiss grid consists of approximately 14 million cells and was generated using ANSYS ICEMCFD (3 000 blocks). The Finnish grid features approximately 15 million cells and was generated using Gridgen (76 blocks, 81 blocks with Sidewinder). FINFLO used the Chimera technology for different flap positions. In the Swiss grid all gaps on moving control surfaces were closed, while they were all open in the Finnish grid. A first series of calculations was made for Swiss design load conditions and aerodynamic forces and pressure distributions were compared. Some differences were observed, which were attributed to the different grids, solution methods and turbulence modeling approaches. The agreement in results was good, especially if one keeps in mind the complex geometry and the complex flow physics.

From the CFD results the structural component loads at reference locations were computed to assess the quality of the simulations. These reference locations correspond to the locations used during the Swiss ASIP study performed by Boeing in St. Louis. Four symmetrical load cases at different points in the sky were selected for this study. The results obtained on both the Swiss and Finnish grids were excellent; some differences were observed at the leading edge and trailing edge flaps due to the different grid strategies in this area (open versus closed gaps). Also the surface grid of both were compared, which showed small differences at several locations. For the next series of calculations the same surface model was used. On both the Swiss and Finnish side improved grids were developed, which consists in the order of 25 million cells for half a model. The old calculations were redone and showed an improvement in results.

Swiss Approach:

The calculations of the Swiss F/A-18 flow field are carried out using the NSMB Structured Multi Block Navier Stokes Solver. NSMB was developed from 1992 until 2003 in a consortium composed of two universities, namely EPFL (Lausanne) and KTH (Stockholm), one research establishment CERFACS (Toulouse) and two industrial companies Airbus France (Toulouse) and SAAB Aerospace (Linköping). Since 2004 NSMB has been developed in a new consortium lead by CFS Engineering and composed of RUAG Aviation (Emmen), Astrium Space Technologies (Les Mureaux), EPFL (Lausanne), ETHZ (Zürich), IMFT (Toulouse), IMFS (Strasbourg), the Technical University of Munich and the University of the Army in Munich.

NSMB employs the cell-centered Finite Volume method using multi block structured grids to discretize the flow field. Various space discretization schemes are available to approximate the inviscid fluxes, among them the 2nd and 4th order centered scheme with artificial dissipation, and 2nd, 3rd and 5th order upwind schemes.

The space discretization leads to a system of ordinary differential equations, which can be integrated in time using either the explicit Runge Kutta scheme or the semi-implicit LU-SGS scheme. To accelerate the convergence to steady state the following methods are available:

- local time stepping
- implicit residual smoothing (only with the Runge Kutta scheme)
- multigrid and full multi grid (grid sequencing)
- pre-conditioning for low Mach number
- artificial compressibility for incompressible flows

The ALE approach is available to simulate the flow on deforming grids. Recently, a re-meshing algorithm was implemented in NSMB to permit the simulation of the flows on deforming grids, as found for example in Fluid Structure Interaction problems. NSMB has no limit on the number of blocks used in a calculation. Block interfaces do not need to be continuous since a sliding grid block interface treatment is available.

The most time-consuming process in a CFD simulation is the generation of the grid. This involves different steps. First (if required) the CAD surface needs to be cleaned up, then a multi block topology needs to be set up, and finally the grid is generated.

The F/A-18 single seat model was the basic configuration for this study. The gaps between the control surfaces were closed for simplification. Important antennas were incorporated. No engine model was used. The turkey feathers of the engine were omitted. Pylons, tanks and AIM-9 and AMRAAM missiles are part of the store configurations.

The latest grid for the F/A-18 fighter was generated by the RUAG Department of Aerodynamics in collaboration with Mindware, using ANSYS ICEM CFD software. The half model grid has 3377 blocks and 14.5 million cells see Fig. 11.

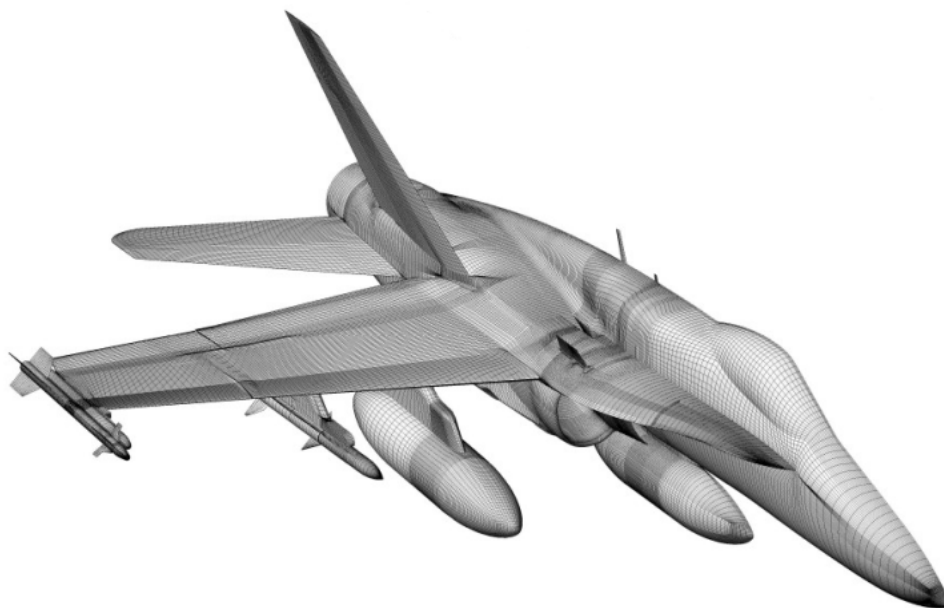


Fig. 11 Detail of the F/A-18 grid (half model).

Finish Approach:

The development of FINFLO flow solver dates back to 1987, when a CFD research project was started at the Helsinki University of Technology. One of the initiators of CFD research was the Finnish Air Force, which needed the right tools and expertise to study aerodynamic loads. Today the Air Force is still one of the main users of the code via Patria and Finflo Ltd. Since 2001, the software has been maintained and developed by Finflo Ltd., a company founded by the developers of the original code. The code is also developed at Aalto University, Lappeenranta University of Technology and VTT Technical Research Centre of Finland.

In FINFLO a structured multiblock grid topology and on a finite-volume technique are used [5, 6]. Geometry modeling is enhanced by a Chimera technique and discontinuous block interfaces, while a multigrid technique is utilized to accelerate convergence. The FINFLO code has been parallelized using the MPI standard to allow it to be run on both servers and multicore workstations. Turbulence modeling using FINFLO can range from $k-\epsilon$ [7] and SST $k-\omega$ models [8, 9] to full Reynolds stress closure. For the solution the following methods are utilized:

- local time stepping
- implicit residual smoothing (only with the Runge Kutta scheme)
- multigrid and full multigrid (grid sequencing)
- pre-conditioning for low Mach number
- artificial compressibility or pressure correction for incompressible flows

The ALE approach is also available to simulate the flow on deforming grids.

One important field where FINFLO has been applied is that of rotating machinery. The code can be used to simulate flows e.g. in pumps, in high-speed compressors, and around ship propellers. The same approach can be utilized in aircraft pull-up simulations by setting the external flow field to rest and putting the grid into a circular motion [3]. The aircraft can be considered to be attached to the end of a whirling arm pivoted at a point somewhere above the aircraft. The angle of attack cannot be modeled in the traditional way, i.e. by manipulating the direction of the external flow. It must be taken into account in the determination of the pivot point location as shown in Fig. 12 Note that the angle of attack is not constant, but increases from nose to tail.

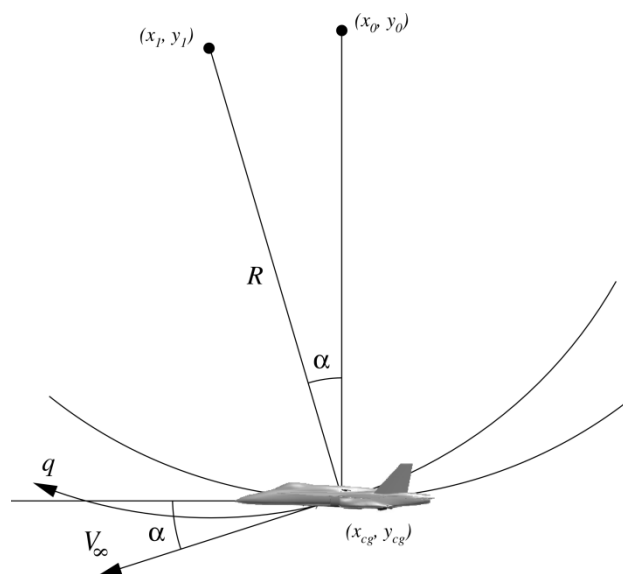


Fig. 12 A definition of the angle of attack as the aircraft is in a pull-up motion.

The radius of the pull-up circle is obtained from

$$R = \frac{V_{\infty}^2}{g(n-1)} \quad (1)$$

where n is a load factor, g the acceleration of gravity and V_{∞} the free stream velocity. The angular velocity q is

$$q = \frac{V_{\infty}}{R} = \frac{g(n-1)}{V_{\infty}} \quad (2)$$

In the present solution system a steady-state simulation can be performed. As a result of the grid motion the aircraft sees the steady flow field as if it were curved (see Fig. 12).

The Finnish half plane F-18C grid consist of 76 computational blocks and the number of cells in these blocks is 13'760'000. With the AIM-9M Sidewinder missile in place, the half plane grid contains 15'873'536 cells in 81 blocks (see Tab. 1).

	Blocks	NOF cells	Surface elements
Base	76 (12)	13 760 000	191 136
AIM-9M	5 (5)	2 113 536	33 024
Total	81 (17)	15 873 536	224 100

Tab. 1 F/A-18C computational grid details. Number of Chimera blocks shown in parentheses.

The surface grid with the wing tip missile is shown in Fig. 13 The overlapping grid structure (Chimera) around movable control surfaces in a wing section is illustrated in Fig. 14. The grid was created using the Gridgen software.

Neither the Finnish F/A-18C CFD model nor the FINFLO flow solver contains any engine models. However, the effects of the engine on the surrounding flow field can be described by defining the flow conditions at locations where the engine (General Electric F404-GE-402) would be connected to the CFD model (see Fig. 15).

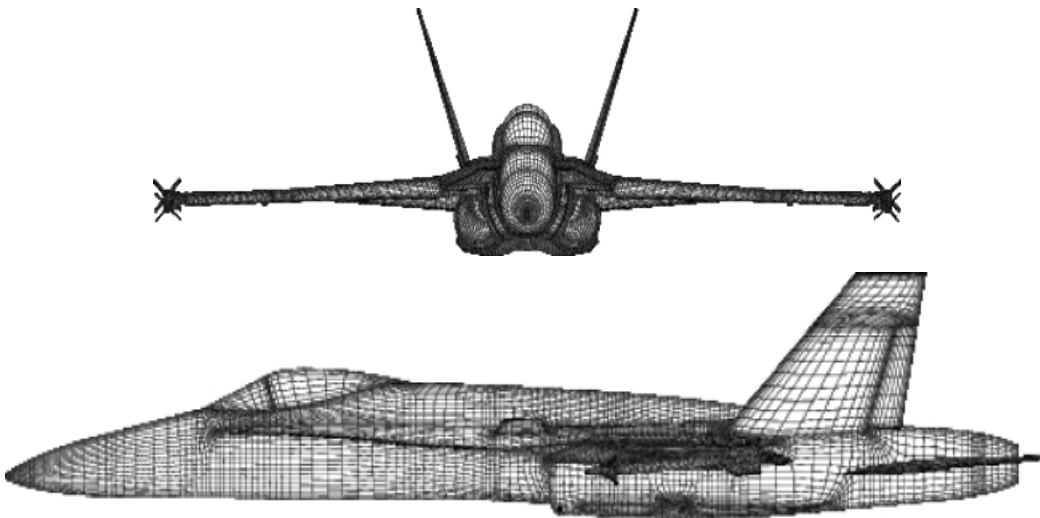


Fig. 13 Finnish F-18C surface grid with AIM-9M (only every other grid line is shown).

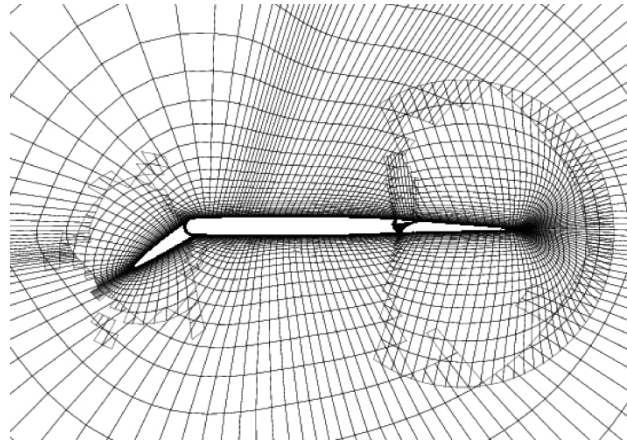


Fig. 14 Chimera blocks around the control surfaces.



Fig. 15 Engine boundary values are defined at the compressor location and at the nozzle inflow location.

The flow conditions through the engine are obtained using a separate computer program provided by the engine manufacturer. In this case the flow situation is interesting only at stations 1, 7, 8 and 9 (see Fig. 16). Flow situations at stations 1 and 7 are used as boundary conditions in the CFD model. The flow solver handles station 1 as an outlet, since the flow comes out of the grid, and station 7 as an inlet, since the flow direction is into the grid. From stations 8 and 9 only the nozzle throat diameter and the engine exhaust diameter are used when manipulating the computational grid. The nozzle adjustment is done in the same grid manipulation program that is used for adjusting the control surfaces. In most cases only the flight altitude and the free stream Mach number are needed for a good approximation of the engine mass flows.

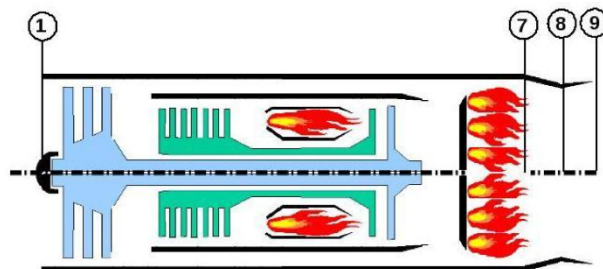


Fig. 16 Engine station diagram.

Results

Before the generation of the grid it was decided to compare the F/A-18 geometry used for the CFD simulations in Finland and Switzerland. Several differences were observed as can be seen in Fig. 12 which shows the two geometries. For example the canopy position was not the same, a difference in LEX fence height was observed and the position of the wing tip

missile was different. Several other smaller differences were found. These geometrical differences were corrected so that the same geometry was used in Finland and Switzerland.

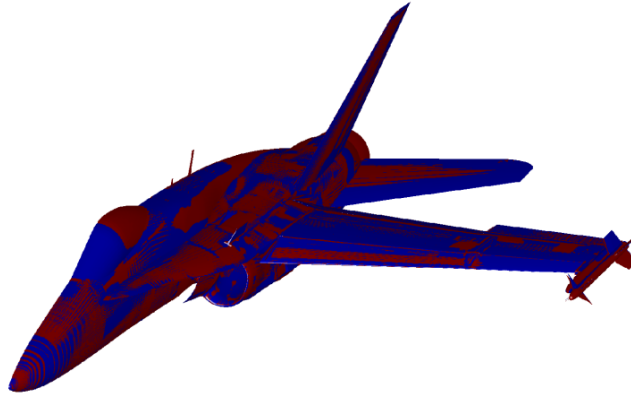


Fig. 17 Red Swiss model, blue Finland model.

The Swiss F-18C CFD grid is fully structured while the Finnish grid contains overlapping blocks (Chimera). The volume grid resolution of the Swiss grid is better than the resolution of the Finnish grid. The nominal first cell height of the Swiss grid is smaller but the cell height stretching is stronger. The radius of the Swiss volume grid is about 250 m while the radius of the Finnish grid is about 500 m.

In the Finnish model also the Sidewinder is modeled using overlapping blocks which makes grid modification very easy.

Several other smaller differences were found. The use of overlapping blocks in the Finnish model requires small gaps between the main wing and the control surfaces. On the leading edge side the gap between the wing and the leading edge flaps is larger than on the real aircraft. On the trailing edge side the gap geometry in the Finnish model is more realistic than the closed geometry in the Swiss model.

However, also in the Finnish model the geometry of the gaps around the trailing edge flaps and shrouds is strongly simplified.

In the Finnish model the engine nozzle shape is adjusted according to the power setting. The difference in the after body modeling will lead to different pressure distributions thus complicating the comparison of after body loads. In general, all the geometry differences found are unimportant when the overall accuracy of numerical flow simulations is considered.

Load Cases:

The load cases were selected from an instrumented Finish aircraft of the MINIHOLM test campaign for structural loads evaluation.

AIM9M	Mach	Altitude	AoA
Yes	0.73	3150 ft	9.6°
No	0.44	8750 ft	25.3°

Tab. 2 Load cases studied.

The Swiss (CH: NSMB) CFD calculations employed the $k-\omega$ -SST and Spalart-Allmaras turbulence models whereas the Finnish (FI: FINFLO) CFD simulations used only the $k-\omega$ model. The following values for C_L (lift coefficient) were obtained:

Mach	AoA	Spalart CH	k- ω -SST CH	k- ω FI
0.73	9.6°	0.750	0.794	0.696
0.44	25.3°	1.331	1.352	1.336

Tab. 3 Computed lift coefficient C_L .

C_p plots were made to understand the differences, and these are shown in Fig. 18 and Fig. 19. It should be mentioned that the gaps between control surfaces are modeled in the Finnish CFD model, while they are closed in the Swiss model. Analyses of the results show a small difference in the position of the canopy shock. But larger differences can be observed on the wing. Fig. 19 shows that the results obtained using the Swiss approach show a larger low pressure region than the results obtained using the Finnish approach. This is probably due to the modeling of the gaps in the Finnish approach. Fig. 19 shows an opposite behavior (a larger low pressure region on the wing with the Finnish approach), but it should be kept in mind that the angle of attack as well as the trailing edge flap deflection angle are much larger for this case.

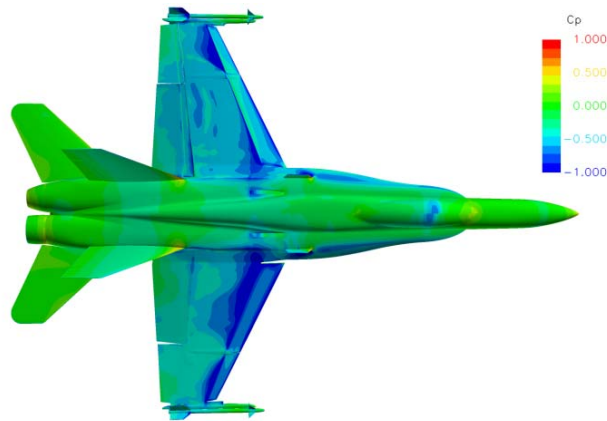


Fig. 18 Top Finland, bottom Swiss load case with AIM-9M.

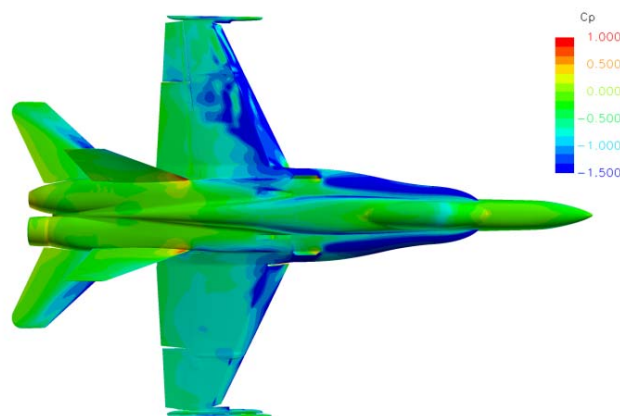


Fig. 19 Top Finland, bottom Swiss load case without AIM-9M.

Sensitivity Analysis of CFD Calculations

All calculations discussed in the previous sections were made using the $k-\omega$ turbulence model. This model was developed for aerospace applications, and in general provides satisfactory results. For highly separated flows, the $k-\omega$ model, and in particular the Menter Shear Stress (MSS) variant has received much attention recently.

Due to the high angle of attack for the 8.25 g steady-state maneuver, large regions of unsteady and separated flow are present. For this reason the C_L convergence histories showed oscillations. One of these 8.25 g manoeuvre was calculated using the $k-\omega$ MSS model, and Tab. 4 summarizes the aerodynamic coefficients and the N_z for the 2 computations. The differences are small, with the computation using the $k-\omega$ model yielding a slightly higher N_z which is closer to the expected value.

Case	C_L	C_D	C_M	com N_z	exp N_z
Spalart	1.287	0.561	0.154	8.06	8.25
$k-\omega$	1.294	0.563	0.170	8.11	8.25

Tab. 4 Aerodynamic coefficients for Spalart and $k-\omega$ turbulence models, 8.25g maneuver.

Small differences in the pressure contours ($p - p_\infty$) can be observed on the upper side of the horizontal stabilizer, on the vertical fin, and on the fuselage downstream of the wing attachment. On the lower side differences can only be observed on the horizontal stabilizer. In the plane at $x = 16$ m (the reference position of the vertical tail) large separated flow regions could be observed, and differences in computed results were apparent, see Fig. 20. However, it should be noted that the flow is unsteady, and differences may come not only from the turbulence model, but also from the unsteadiness of the flow.

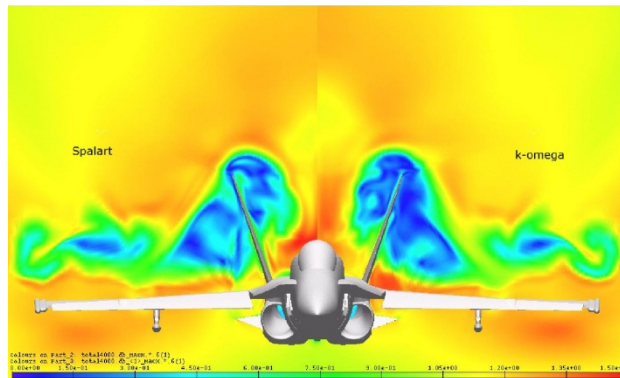


Fig. 20 Comparison Mach contour plot of Spalart and $k-\omega$ -SST turbulence model.

Besides the influence of the turbulence model, the influence of the Mach number, of the angle of attack (AOA), and the deflection of all control surfaces on the F/A-18 were analyzed. The change of the angle of attack (AOA) was very remarkable because it affects the lift of the aircraft. A difference of only 1° in angle of attack may change the C_L value by 20%. The same change in the deflection angle of the control surfaces showed only a small influence on the aerodynamic coefficient C_L , C_D , and C_M .

The influence of a change of the Mach number in the order of 0.02 showed for the aerodynamic coefficients a very small impact of 2% which is within the order of the accuracy of the CFD computation.

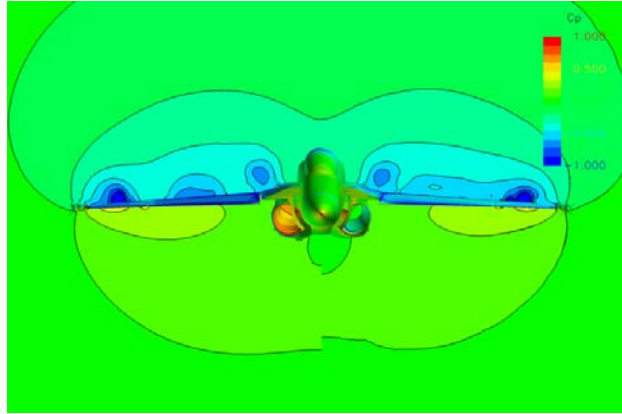


Fig. 21 Pressure coefficient obtained using the FINFLO solver on different grids (Swiss grid on the left, Finnish grid on the right), Mach=0.73, x=12.5m.

The Swiss grid and the Finnish grid were processed with the FINFLO solver to study the differences. In general a fairly good agreement between CFD results concerning the component loads and even differences in the flow field were observed, see Fig. 21.

Structural Component Loads

For the structural analysis the loads of the aircraft on the different components and the different sections are of prime interest. Fig. 22 shows the sections, the reference axes and points where these loads are calculated for comparison. The aircraft was split into two sections on each wing, two sections on the fuselage, one section at the root of each control surface and a hinge axis for each flap.

In the Fig. 23 the partition of the aircraft surface used for the CFD calculations is represented. Every structural element has been taken into account, so that accurate quantitative comparisons between different simulations and between CFD simulation and flight testing can be done. Of course for the flight loads the inertia loads have to be subtracted before the comparison can be made.

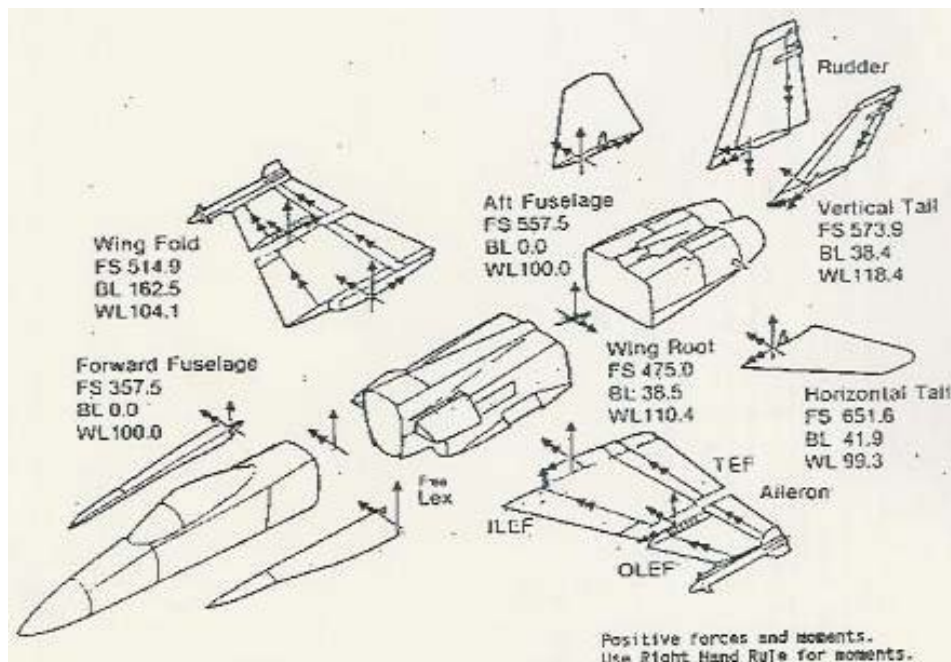


Fig. 22 Reference locations and sign convention.

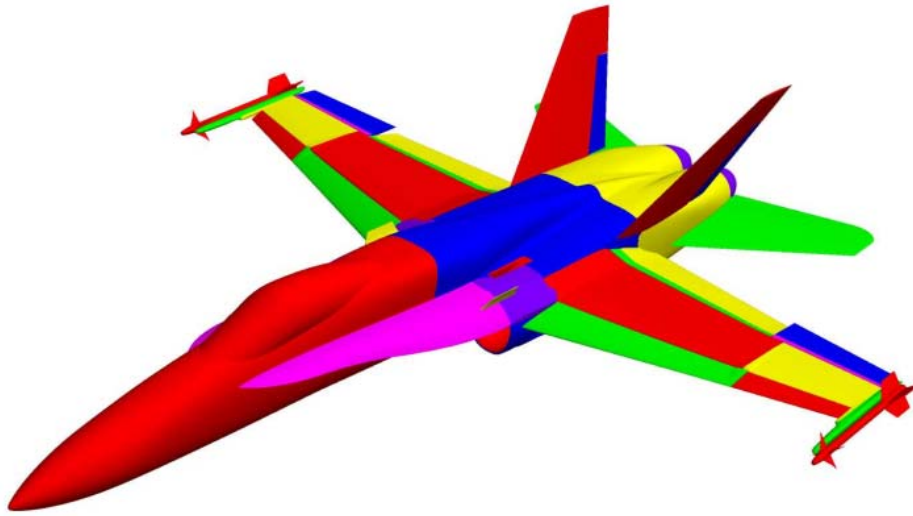


Fig. 23 F-18 surface division into components.

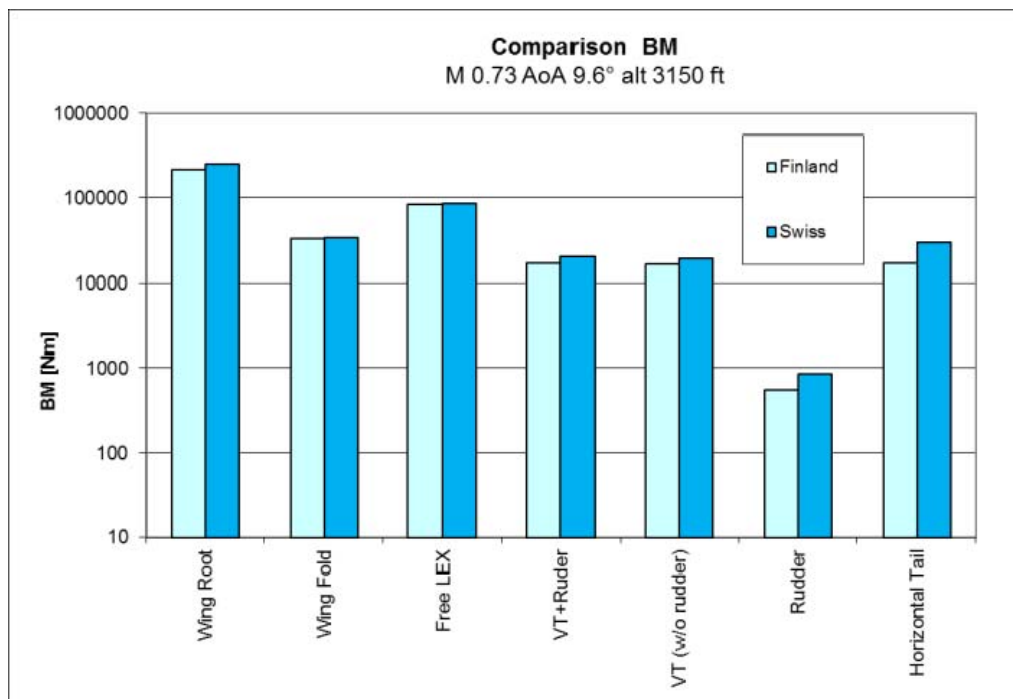


Fig. 24 Bending moment on aircraft components.

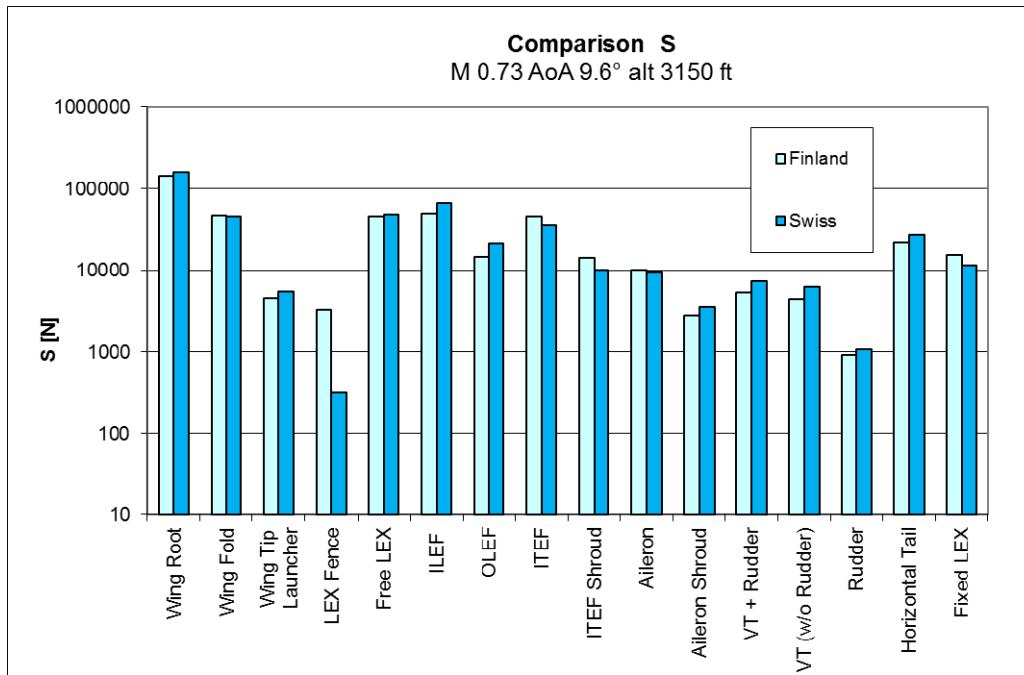


Fig. 25 Shear forces on aircraft components.

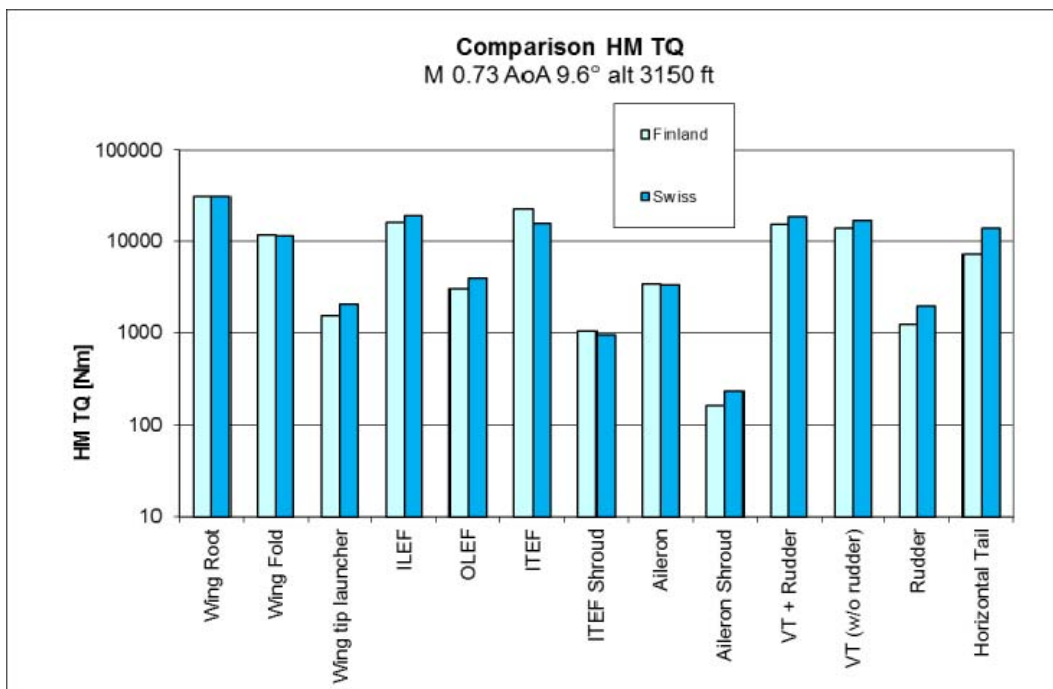


Fig. 26 Hinge moment or torque on aircraft components.

Fig. 24 to Fig. 26 show the comparison between the Finnish (FINFLO) and Swiss (NSMB) grid/solver for the different component loads. A logarithmic scale on the absolute values is used in order to be able to put all the components in the same diagram.

Both simulations give bending moments in very good agreement for the wing, quite good for the vertical tail, but they show differences for the horizontal tail (40%). We also observe that Swiss (NSMB) bending moments and the corresponding shear forces are systematically higher than those of Finland (FINFLO), with the exception of the wing fold, where the shear is lower. This fact indicates that the center of pressure of the outer wing is more outboard in the Swiss CFD calculation.

For the vertical forces the agreement is also quite good to good. We observe that the big differences concern mostly the small components like the LEX fence, the rudder and the shroud, which are very sensitive to the local flow conditions and to details of the grid generation (see Fig. 27). The same remark holds for the comparison of hinge moment and torque.



Fig. 27 Geometry comparison in four wing sections

Other sources of differences worthwhile to mention are:

- The position of the vortex generated by the free LEX and of the flow separation, which are detrimental for the forces of the components in the rear part of the aircraft, can be principally attributed to the higher angle of attack.
- The use of different turbulence models and different flow solvers also has an influence on the results.

Conclusion & Outlook

In addition to the open cooperation, a spirit of healthy international competition has contributed to model and method improvements in both countries. Both sides have improved their models and developed their post-processing capabilities. Both sides have benefited from geometry and control surface hinge line comparisons. In the newest Finnish model the cabin (canopy) location is fixed according to the information received from Switzerland. Similarly, the Swiss side is improving the Sidewinder location and the LEX fence size.

The collaboration is very unique and provides a great opportunity to improve the complex CFD calculations on the F/A-18 aircraft.

Both countries will profit from this effort which is much more than just research in the field of advanced CFD calculations. The advantage provides a considerable improvement in grid strategies and numerical simulation for accurate maneuver loads prediction including unsteady flows.

The aim of the cooperation is a situation where all numerical simulations done in either country could be used by both sides.

4.7 Development of new Grid for F/A-18 CFD Loads Calculations

M. Guillaume, A. Gehri A. Hauser. P. Stephani / RUAG Aviation, D. Charbonnier, J. Vos / CFS

Introduction

A 1st generation of F/A-18 grid was used in the period 2002 - 2006. This grid had about 7 Million grid points (with only 11 cells in the boundary layer). Many aircraft details (antenna, gaps between components, AIM9, ..) were not modeled.

A 2nd generation of F/A-18 grid was used in the period 2007-2012. This grid had about 14 Million grid points (with about 16 cells in the boundary layer). This grid included all aircraft details, but had the following shortcomings:

- the grid resolution
- modification of aircraft components (control surface deflections, add/remove fuel tanks, launchers, etc)

A 3rd generation F/A-18 grid was build in 2012 to remove the shortcomings of the 2nd generation grid. Target number of grid points: around 25 Million.

Strategy Grid Generation

Two mesh strategies were investigated on a simplified configuration:

1. Patch grid approach – each components is placed in a box with a sliding block interface around
2. Chimera approach – each component has its own grid, need to have an algorithm to detect overlapped cells

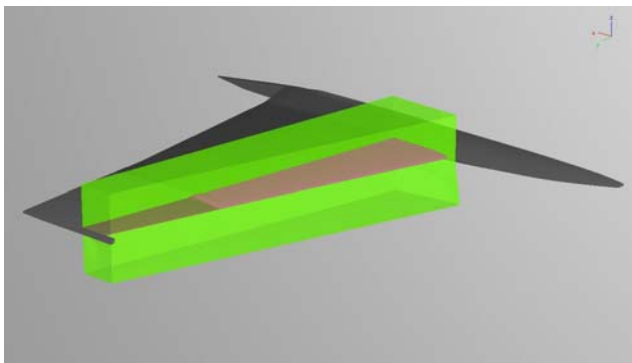


Fig. 28 Chimera

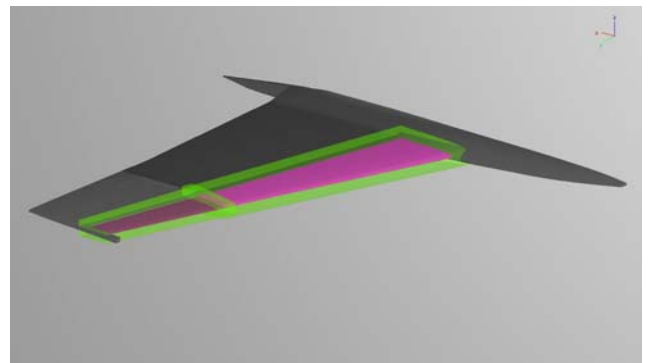


Fig. 29 Patch Grid

Patch grid approach requires geometry and mesh topology modifications for large control surface deflections. Gaps are not modeled.

Chimera approach has the required flexibility to change quickly control surface deflections, add/remove components. Mesh quality is better compared to patch grid approach

But the chimera approach requires an investment in the inhouse NSMB CFD solver technology to improve the chimera method available in NSMB

Conclusion

Decision was made to use the Chimera approach for the 3rd generation F/A-19 grid because this approach provides the necessary flexibility and yields a higher mesh quality.

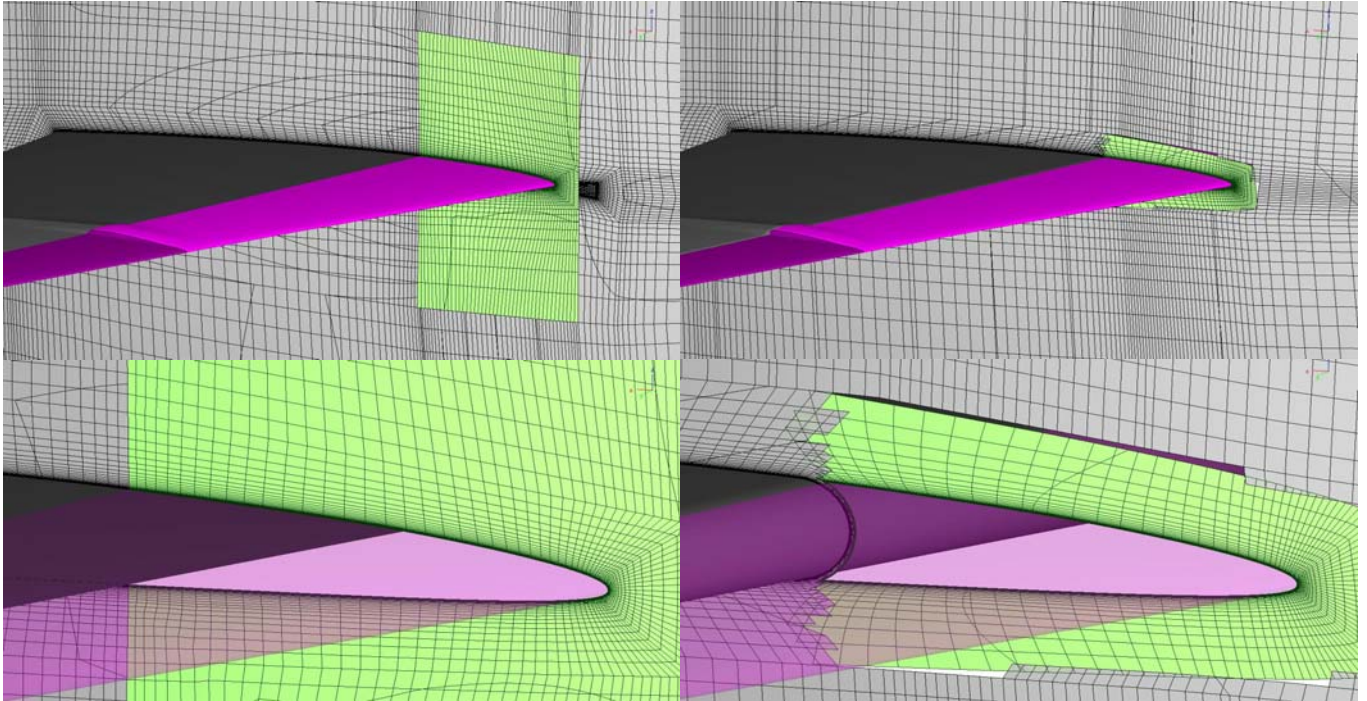


Fig. 30 Examples of Patch (left) vs. Chimera grid (right).

Chimera solid Components

An important task was the definition of the solid components for the Chimera application. This needs already some experience due to the grid design and compatibility.

The following components were selected:

Chimera parts	Surface cells	Volume cells	Number of Blocks
ILEF	16'400	1'050'000	28
OLEF	12'000	770'000	28
TEF	15'400	800'000	14
TEF SHROUD	13'600	760'000	14
AILERON	12'700	660'000	26
AILERON SHROUD	9'700	500'000	6
HSTAB	22'400	1'670'000	30
RUDDER	5'700	300'000	10
S5 SUU-62AA	3'300	160'000	5
S5 TANK 330	6'700	380'000	8
S9 AIM-9X	20'000	1'270'000	328

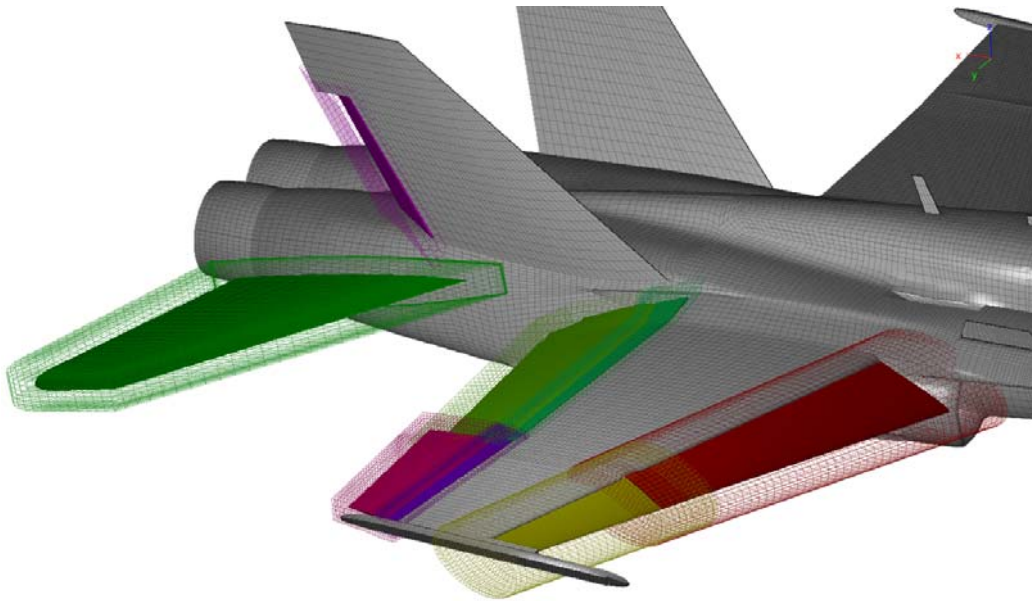


Fig. 31 Details of Chimera mesh on wing, horizontal tail, vertical tail.

Lessons Learned

After more than 10 years working on CFD for the F/A-18 we figured out what must be improved to get accurate results for static and fatigue loads calculations. Accurate CFD calculation is a very powerful tool for structural loads generation especially to study the impact of new missions and configurations on the structural integrity.

The number of grid points is twice higher than foreseen, but

- Grid quality is very good, boundary layer is well resolved, grid orthogonality much better compared to 2nd generation grid
- No regions with large cell spacing
- Boundary layer resolved in gaps
- Requirements for grid spacing used in AIAA workshops (Drag prediction, high lift, aero-elasticity) respected

A large number of improvements were made in last years to the Navier Stokes Multi Block (NSMB) CFD solver:

- Detection overlapping cells improved (problem of solid cells in fluid and fluid cells in solid)
- Memory requirements improved (from 4Gbyte/proc to 2Gbyte/proc)
- Overlapping cells near block interfaces improved and parallelized

Further improvements are possible: reducing further the memory requirements in the chimera initialization process, improvements in the interpolation process and improvements on the use of ghost/buffer cells.

With the improvements of the NSMB solver managed by CFS in Lausanne and the 3rd generation grid better results for loads prediction will be possible. This will allow us to handle new missions and external configurations for the future life assessment of the Swiss F/A-18.

4.8 Investigation of Ex-Military Planes under civil Usage

M. Guillaume / ZHAW, A. Uebersax / RUAG Aviation

Introduction

Since many years old military planes of the type Pilatus P3 (trainer) and Jets of De Haviland Vampire and Venom are in civil operation so called annex II planes with civil registration HB.

The federal Office of Civil Aviation (FOCA) would like to know the fatigue limitations due to aging and the different operation under civil environment.

For the former military usage of the fleet aircraft, limited usage data is available in the form of cumulative Nz exceedances per 1'000 flight hours (FH). Only a few airplanes out of the Pilatus P3, Vampire and Venom fleets were equipped with fatigue meters (Nz exceedance counters).

For the P3 a Swiss full scale fatigue test was performed in 1960 with the last production plane.

For the Vampire (DH-110) only data from De Haviland was available but for the Venom (DH-112) a Swiss full scale fatigue test was performed, several wing pairs were tested over 3 periods from 1963 till 1976.



Fig. 32 Pilatus P3 airplane



Fig. 33 Pilatus P3 test set up



Fig. 34 Vampire DH-110



Fig. 35 Venom DH-112

Compared to the Vampire, the Venom featured a new wing with a laminar flow profile, a more powerful engine and was built from the new aluminum 7075-T6 alloy. As well, the Swiss Air Force usage showed to be much more severe for the Venom than for the Vampire.

The safe life was only 500 FH. The goal of the Swiss was to perform more than 1'000 FH with the Venom and demonstrate a safe operation and address necessary structural improvements as early as possible.

Pilatus P3 Test

For the P3 test fatigue history simulator developed by Jürg Branger was used. Based on simple assumptions a flight by flight spectrum was established without any monitoring of the actual fleet. The spectrum block consists of 250 FH with 1056 different flights. Overall 5'000 FH were simulated which was twice the service life. During the test minor damages were observed such as fretting on wing sub-spar jo-bolts, also some stringers showed cracks.

At the end of the fatigue test an ultimate static strength test was added. The specimen failed at 8G while ultimate load would be 9Gg. The failure occurred by shear in the web plate of the main spar in both outer wings, at the attachment to the inner wing due to heavy fatigue damage.

All the P3 aircraft were fitted with a redesign. In 1980 a fatigue assessment was done to set the limits for the usage based on the test results. A 95% level a safe life of 3'000 FH and 12'000 flights was fixed. The P3 fleet leaders have reached over 4'000 FH and 4'800 flights. The civil usage is under investigation. No monitoring data and strain gauge results from early tests are available which is a real challenge for the current life assessment.

Venom Test

From 1963 till 1970 a first test was performed used actual Swiss usage data. Only the primary structure was tested including for the first time ground cycles, which seems to be very important. Overall 25'000 FH were simulated and 3 wing pairs were tested. The test results allowed the Swiss to increase the safe life from 500 to 1'500 flight hours.

After 1970 the Swiss Air Force introduced new missions to increase the tactical capabilities. This showed immediately an increase of the Nz spectrum which was more severe than the Swiss test spectrum. Therefore it was decided to test again the Venom with an updated actual usage spectrum. From 1974 till 1976 additional two wing pairs were tested overall more than 70'000 flights were simulated from 1963 till 1976. Several redesigns were introduced into the fleet. In 1979 more than 50% of the fleet had cracks in the wing spar and inspection were done every 100 flights to ensure a safety by inspection philosophy.

At the moment any airplane is in civil use in Switzerland. The most critical component is the engine due to spare parts and short inspection. This leads to very high costs for keeping such an old plane flying.

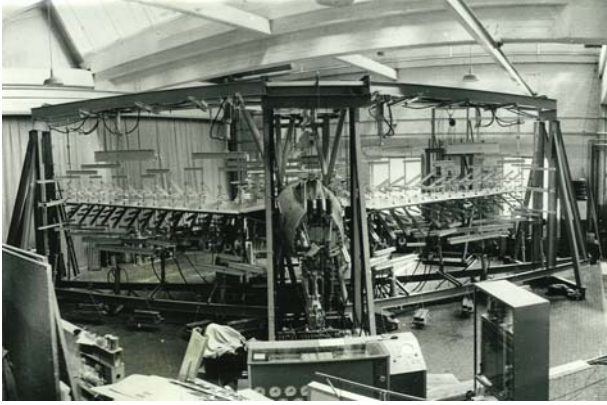


Fig. 36 Venom DH-112 test set up



Fig. 37 Venom DH-112 test set up

Currently all the test data for the P3 and Venom DH-112 is reviewed. Also the improvements and structural changes in the fleets under military usage were assessed.

The next step is to understand the civil usage and to check the current inspection documents which should reflect the results of the Swiss full scale fatigue tests. The goal is define safe life limits for civil operators.

4.8 F/A-18 Structural Activities Master Plan

D. Schmid, C. Kunz, M. Weber, A. Del Don, I. Kongshavn, R. Nebel, A. Gassmann, M. Nastaj, B. Bucher / RUAG Aviation

Introduction

The objective of the Structural Activities Master Plan (SAMP) is to summarize the necessary engineering tasks (ASIP task V) concerning the aircraft structure to guarantee a safe and economic operation of the Swiss F/A-18 Fleet.

RUAG structural engineering has been working since 2011 on the Swiss “F/A-18 Service Life Assessment Program” (SLAP). Critical locations of the F/A-18 structure are being analyzed in detail to determine whether damages can be expected until the end of service (in the year 2030). The goal is to have a recommendation for every critical location by the end of 2014.

Collection of Damage Information

Due to the complexity of the F/A-18 structure, it is not possible to examine the whole aircraft for critical locations and to check every suspicious area in detail. Therefore the search was narrowed down to locations where cracks have already been found. Several sources of information are available. The most important source is the Swiss F/A-18 Full Scale Fatigue Test (FSFT). This test was accomplished at RUAG between 1998 and 2007. The whole F/A-18 structure was used in the test and 10'400 flight hours were simulated. After the test, an extensive tear down inspection (TDI) was made. The structure was disassembled and inspected for cracks. As a result, about 340 nonconformance reports (for cracks, delaminations, etc.) were written during the test performance and at the TDI. During the TDI, many fatigue analyses were performed, however the majority of the cracks found during the test were not analyzed.



Fig. 38 Swiss F/A-18 Full Scale Fatigue Test

International meetings with other operators such as Canada, USA, Finland and Australia are also important forums for the indication of potential critical locations. Most aircraft of these countries have accumulated many flight hours and therefore allow a realistic view of the future of the Swiss fleet. The final source of information to consider is any damages that have occurred already during operation of the Swiss fleet.

Structural Activities Master Plan

There are currently about 400 possible critical locations on the list to be considered and every year about 10 to 20 new locations are added. To analyze every location would be an effort that is not justifiable. Therefore it was necessary to prioritize the locations and the Structural Analysis Master Plan (SAMP) was created. Every potential location was assessed according to the following criteria:

- Effectivity: Can the damage potentially affect the Swiss fleet?
- Frequency: How often was the damage found?
- Criticality: What is the impact of a crack?
- Inspectability: Is the damage easy to inspect?
- Fleet availability: How long will the aircraft be out of service for a repair?
- Economics (Maintenance): How much will a repair cost?
- Swiss-FSFT: Was the crack found in the Swiss FSFT?

Evaluation								
ITEM	0	1	2	3	4	5	7	10
1 Effectivity		x						
2 Frequency						x		
3 Criticality								x
4 Inspectability			x					
5 Fleet availability				x				
6 Economics (Maintenance)				x				
7 CH-FSFT				x				

Fig. 39 SAMP Evaluation Matrix

As a result of this priority matrix, 83 areas covering 150 locations were selected for study between 2011 and 2014. These locations are not likely to meet the Swiss service life requirement of 5000 SFH safe life. For each location, a future study can include an analysis, a configuration comparison, the planning of an inspection, etc.

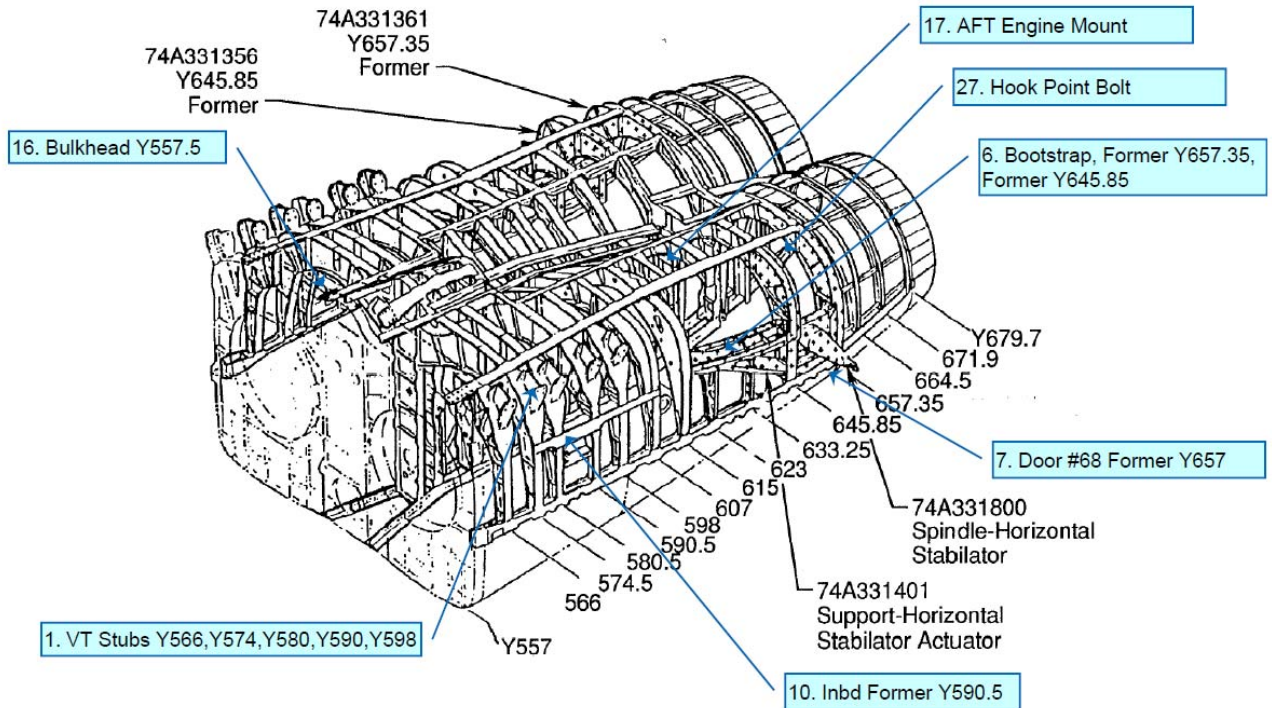


Fig. 40 Locations to be assessed in the aft fuselage

Analysis of the Damages

Different methods are available at RUAG to analyze the damages to understand possible causes and their impact. Finite element analysis and quantitative fractography are used for many locations to determine a crack initiation life.

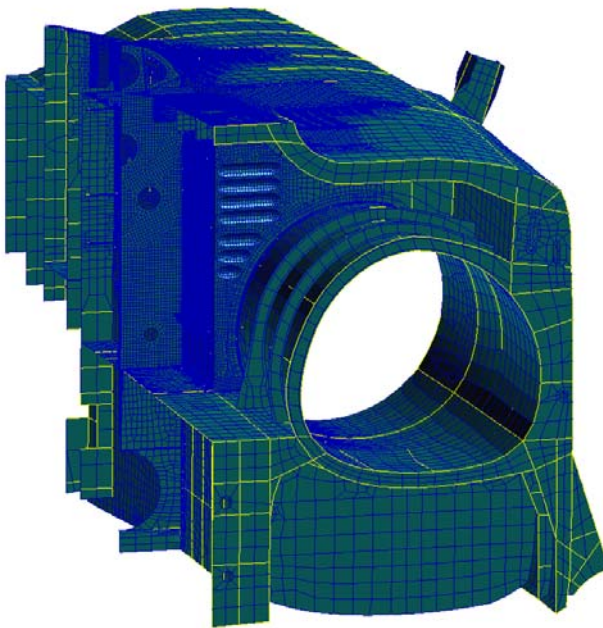


Fig. 41 Finite Element Model

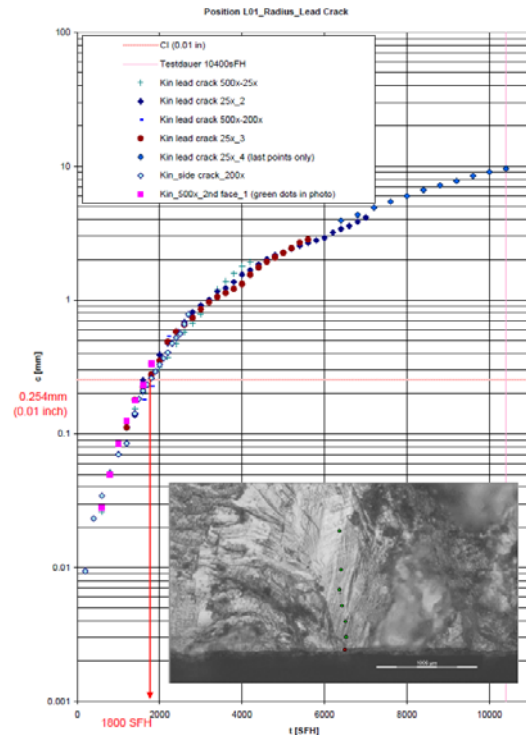


Fig. 42 Quantitative Fractographic

Once the remaining fatigue life is determined for each location, it will be recommended to:

- Use as is (the part meets the design requirement of 5000 SFH safe life)
- Define a safety by inspection concept
- Develop a preventive modification
- Develop a repair (if cracks are already expected)

Way ahead

After the completion of the SLAP in 2014 the proposed repairs, preventive modifications or inspections will be developed in detail. Depending on the number and the locations of the recommended preventive modifications, a second Structural Refurbishment Program (SRP) may be required.

4.9 Quantitative Fractographic Analysis of Swiss F/A-18 D Full Scale Fatigue Test Locations

I. Kongshavn, R. Zehnder / RUAG Aviation, C. Huber / ZHAW, S. Barter / Defence Science and Technology Organisation (DSTO)

Quantitative Fractography (QF) is being used to measure the crack growth curves of critical locations on the Swiss full scale fatigue test (FSFT) article. Starting in 2008, considerable effort has been invested in building up the equipment and expertise for QF analysis in-house, with the support of DSTO (Dr. S. Barter and his associates). By quantitatively measuring the progression of markings on the fracture surface using a light microscope with high quality long working distance lenses, a 'complete' life curve from very small crack sizes (on the order of 0.01 mm) until failure is measured. This 'total life' curve is interpreted as representing both the 'crack initiation life' (CI life) and the 'crack growth life' (CG life), as defined by the OEM. The results are used to correlate or 'peg' the analytical CI and CG lives to the measured QF CI and CG lives via the local stress concentration ($Kt\sigma$). For a more detailed explanation of the QF method, the reader is referred to the numerous publications by DSTO [1], [2].

QF analysis has been carried out on 7050- and 7075- aluminium parts of the Swiss FSFT article, typically at fastener holes and radii. An example is the analysis of the relatively large crack in the ILEF lug (outboard set #4), made of Al 7050-T736. During the FSFT, the earliest cracks were detected non-destructively after 3000 TFH and complete failure of the lug occurred at 9400 TFH. The wing root bending moment spectrum is the principle driver of the fatigue cracking. This spectrum created a reasonably well-marked pattern of progression marks on the failure surface. Starting from etch pits left by the IVD process, which suggested an equivalent pre-crack size (EPS) of 0.016 mm, a complete QF curve could be measured until part failure at a crack size of 113 mm. The crack grew at first exponentially until reaching the carbon skin after approximately 6 mm, whereupon load shedding occurred and the growth rate was reduced to linear.

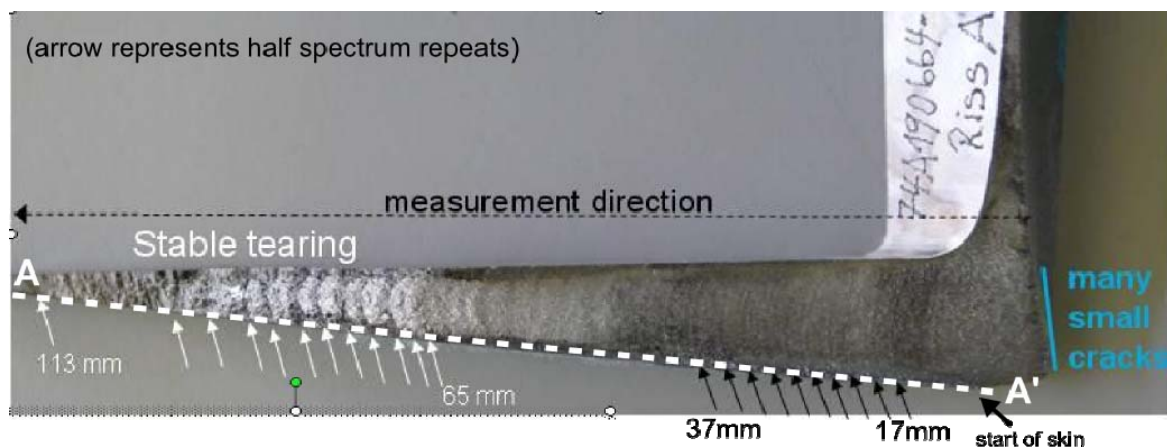
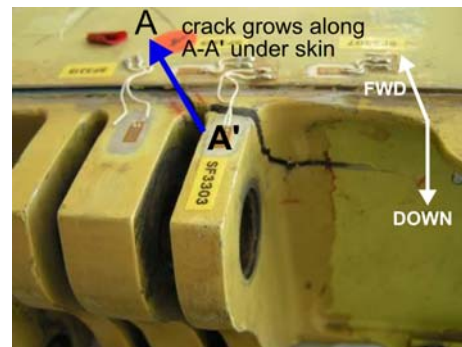
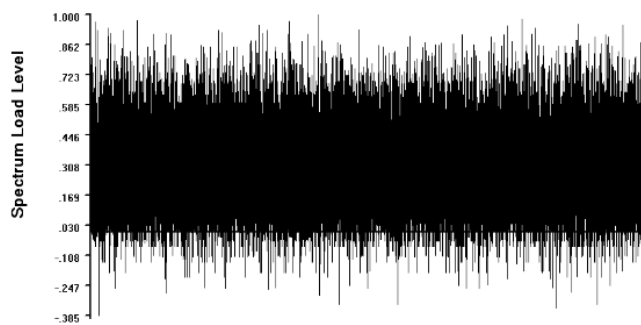


Fig. 43 ILEF lug failure surface showing some repeat markings used for the QF analysis (arrows).

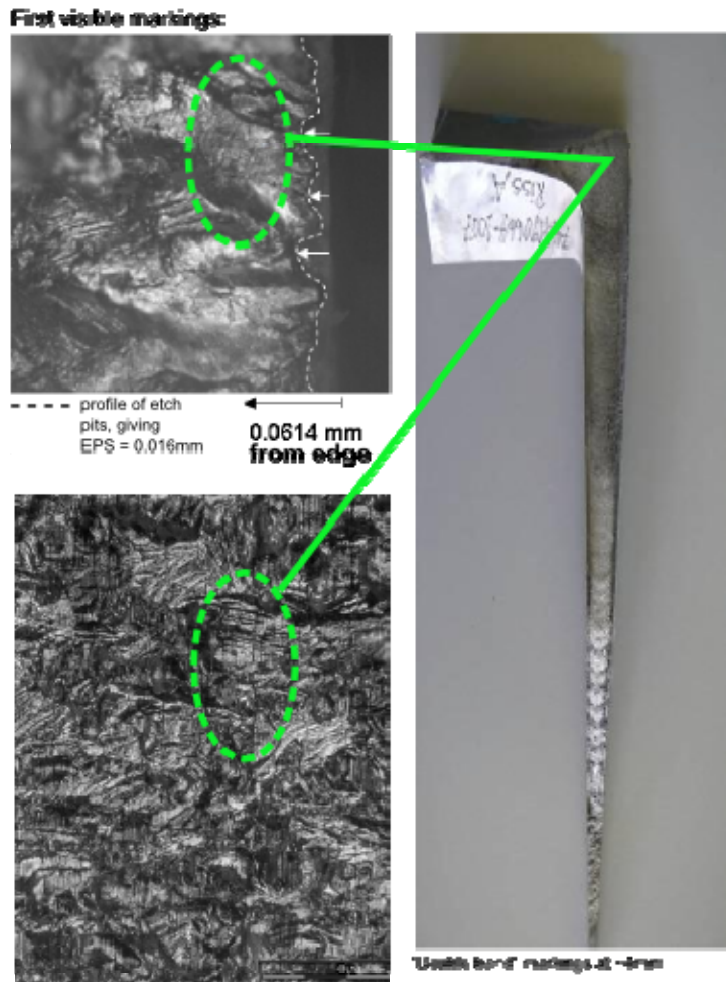


Fig. 44 Close-up of the first visible markings near the origin and at circa 4 mm from the origin.

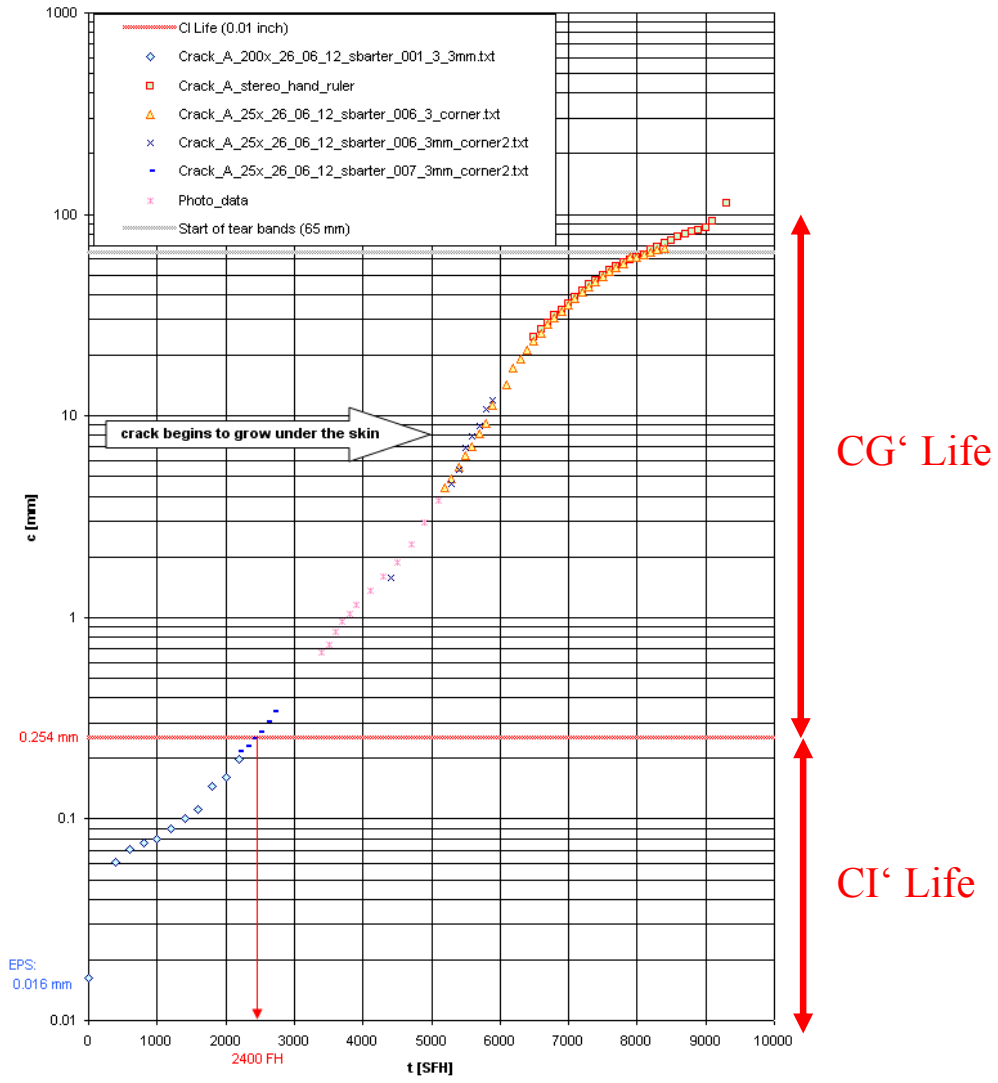


Fig. 45 QF curve of the ILEF lug.

5.0 Evaluation of Marker Loads for Variable Amplitude Spectrum Coupon Test

A. Uebersax / RUAG Aviation, C. Huber, H. Hesselbarth / ZHAW

Introduction

Often crack growth measurements during fatigue tests are complex and of limited accuracy. Therefore, post-test Quantitative Fractography (QF) is an effective method of assessing the crack growth behaviour. The readability of the fracture surface can be highly facilitated by introducing fracture surface markers.

The goals of this work were to gain basic knowledge for the introduction of marker loads in test spectra and to generate a test spectrum based on a mini-Falstaff spectrum that will be used for crack growth testing of aluminium 7075-T7351 alloy open-hole dog-bone coupons. The mini-Falstaff spectrum [3] is optimized for testing. Its loads are not self-marking enough, so that they would be reliably readable, [2]. Therefore, marker loads should be added to the spectrum for subsequent QF evaluation. For the layout of the marker loads, the paper [2] was used as a general guideline.

Approach

Eight different marker load spectra were defined and tested using the following strategies for marker loads: reordering, over- / under-loads and constant amplitudes. Those spectra were compared to the baseline mini-Falstaff spectrum and rated according to the following criteria:

- Visibility/readability of the marker loads over the entire crack length
- Difference in fatigue life compared to the baseline spectrum
- Width of the markerband on the fracture surface compared to the one of the baseline spectrum
- Secondary effects, e.g. differing critical crack length

The different marker load spectra have been developed in sequence, so that the results could be used for the development of the subsequent spectrum, see process in Fig. 46.

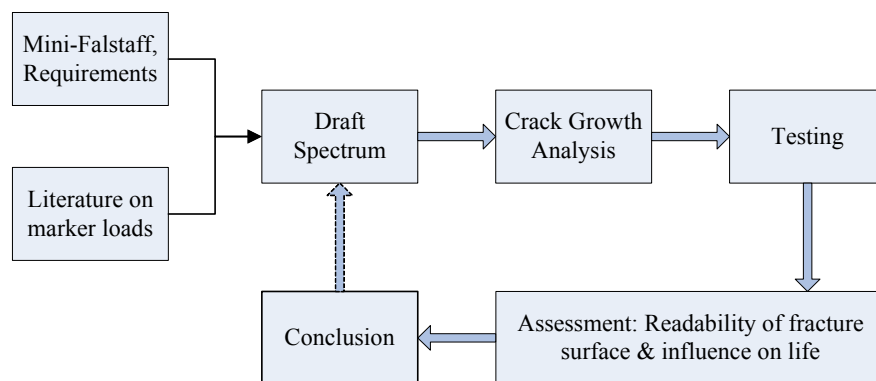


Fig. 46 Marker load spectrum development process

The following equipment was used for the QF evaluation:

- Microscope Olympus BX41M (magnification: 25 to 500-times)
- Stereomicroscope Leica MX8 (magnification: 5 to 60-times)

- REM Zeiss SUPRA 40VP

For each spectrum, the crack growth life was calculated by using a linear elastic fracture model (Willenborg model in AFGROW). The analytical results were compared to the test results. In general, the modelling showed the trends, but was not sensitive enough to allow for a prediction of the exact influence of the marker loads. However, for two similar spectra, the analysis could reliably predict which one shows a crack growth life closer to the baseline spectrum.

The finally developed mini-Falstaff spectrum with marker loads should be used in the project "Effect of Corrosion on Structural Integrity of an Aluminum Wing Lower Skin of a Fighter Aircraft", where coupons with different corrosion levels will be tested. Corroded coupons may show equivalent initial damage sizes that are 10 times larger than for the non-corroded coupons [4] and may show as well an increased net section stress, due to material loss. Crack growth calculations showed that the crack growth lives will vary between 20 to 50 spectrum blocks, depending on the damage size of the coupons. Because of the relatively small minimum number of blocks, it is required that marker loads are added to each spectrum block. Assumed that the first five marker bands will not be readable, 15 to 45 marker bands will remain for the evaluation of crack growth.

Two different net section stress levels (σ_{ref}) were used. 32.3 ksi is the actual stress at the reference location on a fighter aircraft wing lower skin. In order to save on testing time, this reference stress was increased to 34.5 ksi for some tests. For the finally proposed marker load spectrum the reference stress was lowered again to 32.3 ksi to guarantee a minimum number of readable marker loads for the corroded coupons in the later test program.

Testing and Results

In total 19 coupons were tested under laboratory conditions (air and ambient temperatures). The test series with multiple coupons showed small standard deviations with a maximum of 6% of the average value.

Group	σ_{ref} [ksi]	No. of Coupons	Total Life				
			Average [blocks]	Stand. Dev.	cycles/block	% of baseline life (blocks)	% of baseline life (cycles)
Baseline 34.5ksi	34.5	3	42.30	2.30	9006		
Markerband_I_Reordering	34.5	3	39.60	2.09	9006	93.62	93.62
Markerband_II_Altuol	34.5	3	24.00	0.00	9011	56.74	56.77
Markerband_III_2R-CA-1	34.5	1	30.61	n/a	9516	72.36	76.46
Markerband_III_2R-CA-2	34.5	1	33.12	n/a	9216	78.30	80.12
Markerband_III_2R-CA-3	34.5	1	33.35	n/a	8961	78.84	78.45
Baseline 32.2ksi	32.3	1	53.12	n/a	9006		
Markerband_III_2R-CA-5	32.3	1	43.12	n/a	9206	81.17	82.98
Markerband_III_2R-CA-6	32.3	1	43.12	n/a	9516	81.17	85.77
Markerband_III_2R-CA-2	32.3	1	45.63	n/a	9216	85.90	87.90
Markerband_III_2R-CA-4	32.3	3	43.10	0.58	9816	81.14	88.43

Tab. 5 Testmatrix with results

Some remarks and explanations to the different marker load strategies are given below.

Mini Falstaff Baseline

Above a crack length of 2.0 mm, the two highest load peaks are clearly visible with a magnification of 25-times and polarisation filter. For a crack length between 0.2 and 0.8 mm an identification of the peaks was judged challenging and between 0.8 and 2.0 mm not

possible. Therefore it was decided to introduce marker loads for the subsequent QF evaluation.

Reordering

A simple option is to reorder the spectrum loads to improve spectrum readability. To achieve a maximum effect with minimal changes, modifications were made to the flights no. 32 and no. 173. The entire flight no. 173 was moved behind flight no. 193 and the four highest and lowest loads of flight no. 32 were combined and moved in front of the highest peak.

The blocks can be clearly distinguished starting from a crack length of 1.0 mm. But the readability of smaller crack lengths is difficult.

Underloads/Overloads

The addition of overloads or underloads is probably the most common strategy for improving QF readability; particularly the addition of overloads. In this work it was tried to combine overload blocks with underload blocks. Overload blocks will most probably result in crack growth retardation, whereas underloads will generally result in crack growth acceleration.

This modification showed an important influence on the fatigue life. The total life of the modified spectrum was roughly 40% shorter than the baseline spectrum. The overloads could not be distinguished from the underloads. A refined version of this strategy would require much more testing to be done.

Constant Amplitude with two different R-ratios

The tests were run with added constant amplitude marker loads with two different R-ratios, one series with $R = 0.5$ and another with $R = 0.7$.

To start with, the number of marker loads was chosen rather high to have a good readability. Measurement of the width of the markerbands for the different numbers of constant amplitude marker loads, revealed a quasi linear correlation between the number of marker loads and the relative width of the marker bands.

Tested constant amplitude marker loads:

- **Markerband III 2R-CA-1:** The following cycles were added at the end of the mini-Falstaff block:
 - 500 cycles with $R = 0.5$ and a maximum stress of 0.8 (in the normalized spectrum).
 - 10 cycles with $R = 0.1$ and a maximum stress of 0.8 (in the normalized spectrum).
 - In order to guarantee the peak-valley sequence, the last valley was lowered to -0.05.
- **Markerband III 2R-CA-2:** Based on the assessment of the preceding spectrum "Markerband III 2R-CA-1", the number of constant amplitude cycles with $R = 0.5$ and a maximum stress of 0.8 was lowered to 200 cycles
- **Markerband III 2R-CA-3:** Based on the assessment of the preceding spectrum "Markerband III 2R-CA-2", the number of constant amplitude cycles with $R = 0.5$ and a maximum stress of 0.8 was lowered to 100 cycles. The marker loads were positioned according to [5]. The 10 cycles with an R-ratio of 0.1 were placed in the middle of the

cycles with an R-ratio of 0.5. Additionally, flight no. 197 was erased from the spectrum to achieve a similar severity as the baseline spectrum.

- **Markerband III 2R-CA-4:** The R-value was raised from 0.5 to 0.7. Additionally the number of marker loads was raised as well. The intension was to reach a relative markerband width of 7% of a spectrum block width.
- **Markerband III 2R-CA-5:** The 10 cycles with $R = 0.1$ were replaced by 50 cycles with $R = -1$. The number of cycles with $R = 0.5$ was 150.
- **Markerband III 2R-CA-6:** Based on the spectrum „Markerband III 2R-CA-4”, the number of constant amplitude cycles with $R = 0.7$ were lowered from 700 to 500.

The advantage of marker bands with an R-ratio of 0.7 against such with an R-ratio of 0.5 was that the markers could be read from a crack length of 0.07 mm until fracture. The spectra with an R-ratio of 0.5 were considerably more difficult to read between crack lengths of 0.3mm to 0.8 mm.

It was discovered that constant amplitude marker bands changed appearance in function of the crack length. For small cracks, until approximately 0.7 mm, the marker bands stand out against the rest of the fracture surface by the different coloration, whereas the marker bands were generally darker than the variable amplitude spectrum. For larger cracks the marker bands could be distinguished from the rest of the spectrum by the change of the surface texture. Therefore markerbands with a larger width are easier to read at this stage.



Fig. 47 Markerband III 2R-CA-4 fracture surface

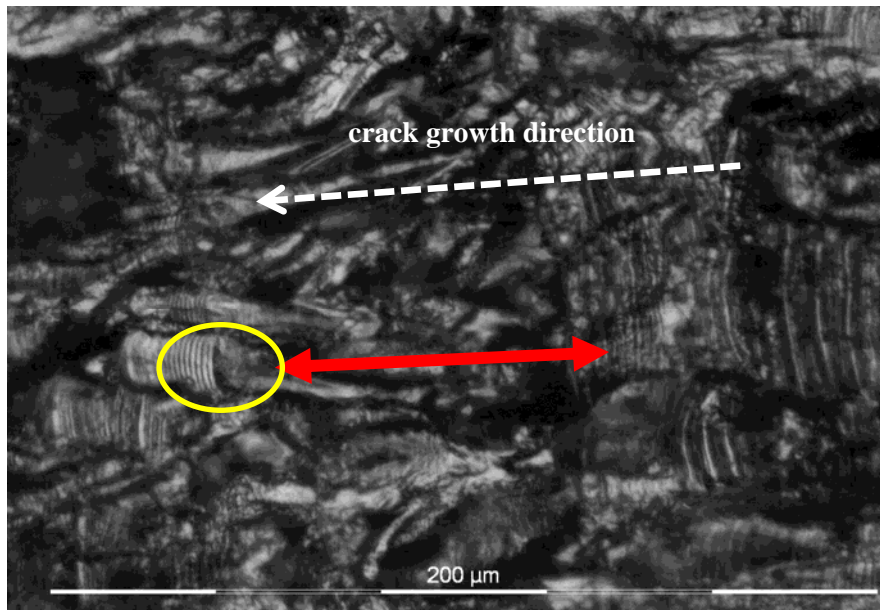


Fig. 48 Markerband III 2R-CA-4: $R = 0.7$ markerband width shown by red arrow, the yellow circle shows the cycles with $R = 0.1$ at 4.4 mm crack length

The test results have shown that the constant amplitude marker loads have the following advantages over the other categories:

- The marker bands are easily readable over the entire crack length (starting at 0.07 mm) if an adequate stress ratio R is used.
- The amplitude of the added load cycles are within the maximum values of the baseline spectrum. Therefore additional local plasticity effects are excluded and the critical crack length remains the same.
- The difference in crack growth life to the baseline spectrum is acceptable.

The following marker load spectrum revealed the best characteristics for the foreseen tests with corroded coupons: *Markerband_III_2R-CA-4*

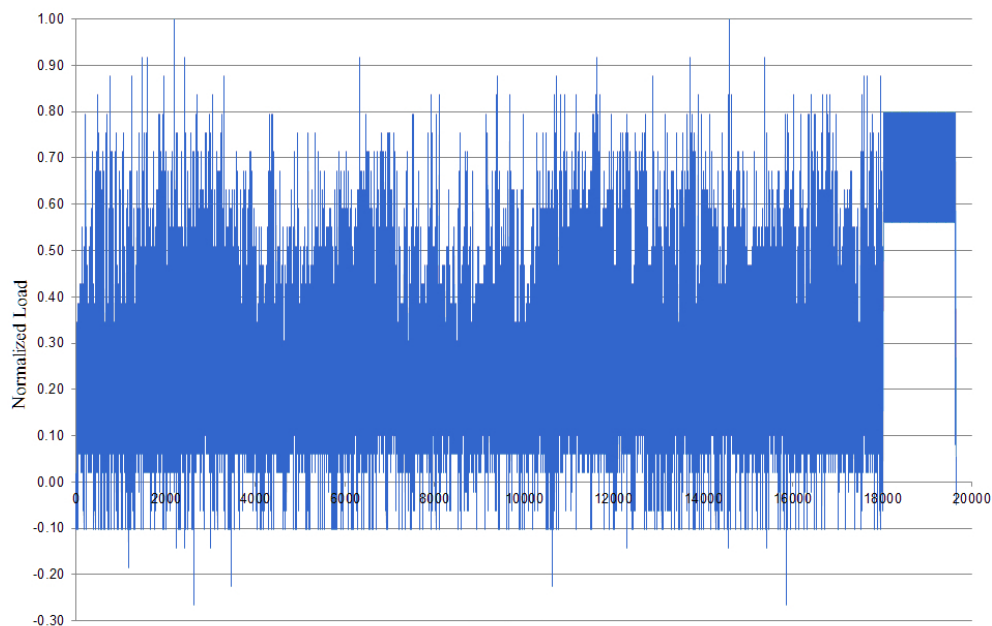


Fig. 49 Road plot of spectrum Markerband_III_2R-CA-4

The spectrum Markerband_III_2R-CA-4 shows the following characteristics:

- The marker bands are easily readable, from a crack length of 0.07 mm to failure of the coupon.
- The total life (in load cycles) is 12% shorter than the one of the baseline spectrum, which was judged acceptable.
- The relative width of the marker bands is 11% of the width of the baseline spectrum block. This should guarantee a reliable identification with slightly different stress levels (corroded coupons).
- The average crack growth rate per spectrum cycle is similar to the crack growth rate of the marker load cycles, see Fig. 50.
- The amplitude of the added load cycles are within the maximum values of the baseline spectrum. Therefore additional local plasticity effects are excluded and the critical crack length remains the same.

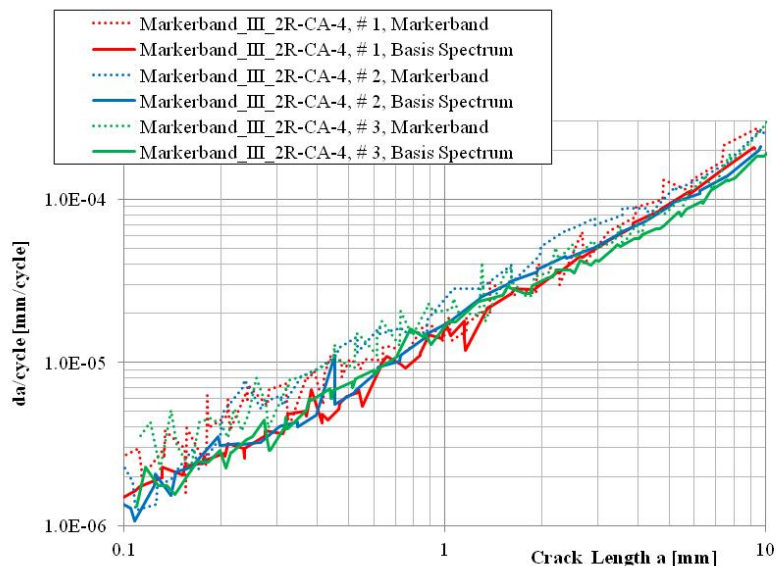


Fig. 50 Similar crack growth rate for markerband cycles and basis spectrum cycles (averaged) for all 3 coupons loaded with the spectrum Markerband_III_2R-CA-4

5.1 Effect of Corrosion on Structural Integrity of an Aluminum Wing Lower Skin of a Fighter Aircraft

A. Uebersax, R. Zehnder / RUAG Aviation, G. Renaud, M. Liao; National Research Council Canada (NRC)

The objective of the ongoing project is to investigate the influence of the presence of exfoliation corrosion and pitting corrosion on the static and fatigue behaviour of an aluminum 7075-T7351 wing lower skin, with a tension dominated fighter aircraft loading spectrum (mini-Falstaff). For this purpose, a combination of static and crack growth analysis models are being developed. Open-hole dog-bone test specimens (see Fig. 51) with specific damages are fatigue tested and used for validating the developed models. The tests are performed on specimens that are pristine, artificially corroded with pits, artificially corroded with intergranular corrosion and repaired by grind-out, see Tab. 6.

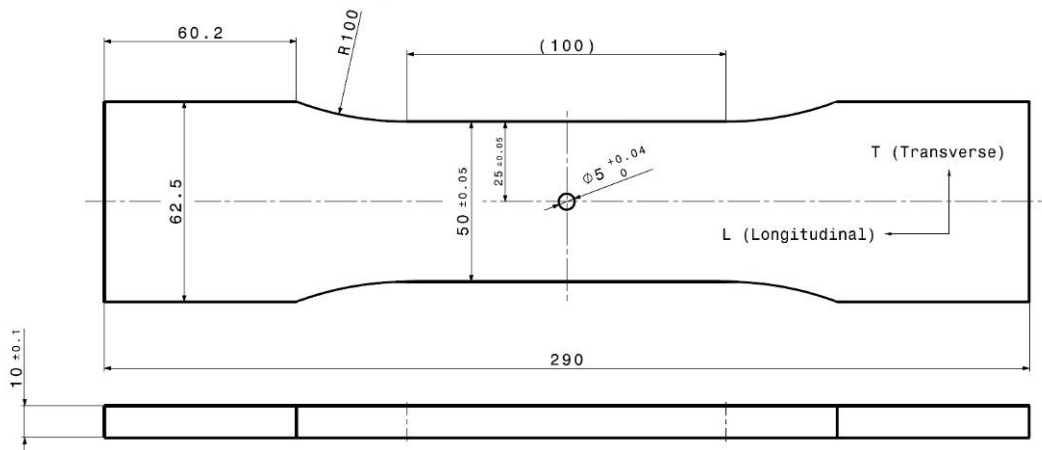


Fig. 51 Definition of the open-hole dog-bone test specimen

Test Series	Damage Size	Number. of Specimens
Pristine	n/a	3
Pitting Corrosion	pitting depth 1	3
	pitting depth 2	3
	pitting depth 3	3
Intergranular Corrosion	corrosion depth 1	3
	corrosion depth 2	3
	corrosion depth 3	3
Grind-out Repair	grind-out depth 1	3
	grind-out depth 2	3
	grind-out depth 3	3

Tab. 6 Test matrix with the different test series

The main outcomes of the project are:

- Better understand the impact of corrosion on the structural integrity of a fighter aircraft aluminum wing lower skin
- Develop engineering approaches and tools for quick assessment
- Help to make cost-effective maintenance decisions regarding corrosion damages

A similar project was finished in 2010 for intergranular corrosion damages on a wing upper skin (aluminium 7075-T651 and compression dominated loading spectrum), see Ref. [6].

This project is performed in collaboration with the Aerospace Portfolio of the National Research Council Canada (NRC).

5.2 Fretting Fatigue Testing and Repair Qualification of a Wing to Fuselage Trunnion

A. Uebersax, I. Kongshavn, A. Gassmann / RUAG Aviation, C. Huber / ZHAW

Fretting fatigue cracking has occurred repeatedly on aluminum wing to fuselage trunnions of a Swiss Air Force F-5E/F fighter aircrafts. The cracks nucleated under the shoulder of the stainless steel bushing in the aluminum fitting due to dissimilar deformation under flight loads. The challenges faced during the development of an improved repair method were the high normal contact stress due to the bolt preload and restrictions arising from the practical application of the repair on the wing. To qualify an improved repair method, a free floating bridge type fretting fatigue test was required. At the start of testing, a universal standard for fretting fatigue testing was not available. Therefore a novel in-house test method with a circular fretting pad was developed.

Combinations of different coating and lubrication were run in comparison to an original baseline configuration. It was concluded that a combination of a hard, abrasion resistant coating on the fretting pad and an additional lubricant were needed to achieve the required life improvement of the 7075-T7351 coupons. The objective was met by qualifying two coating / lubrication combinations that showed a life improvement of at least 2.57 until testing was stopped without any indications of cracking. If a simple log-linear approach is used to estimate the life until coupon failure, this life improvement factor increases to 5.1. It was concluded that the ADLC and Molykote® D 321R combination should be adopted for the final repair solution of the Swiss Air Force F-5 fleet due to its significant improvement in fretting fatigue life, combined with the lowest risk of being worn away.

It was also concluded that the novel free floating bridge type test set-up with circular rotating fretting pads described in the paper [7] offers a more cost-efficient, yet adequate, test method for qualifying fretting fatigue repairs. An improvement to the test set-up has also been proposed, which provides a more exact alignment of the fretting pads and avoids torsion on the rig by a self-centering chock system.

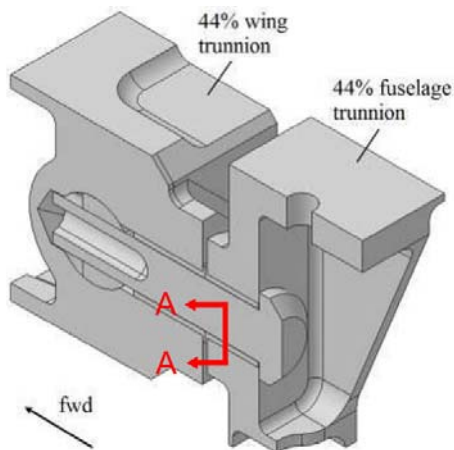


Fig. 52 Structural situation: Pre-tensioned steel bolt transferring shear loads.

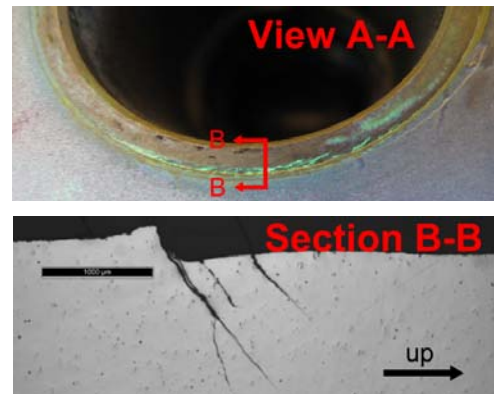
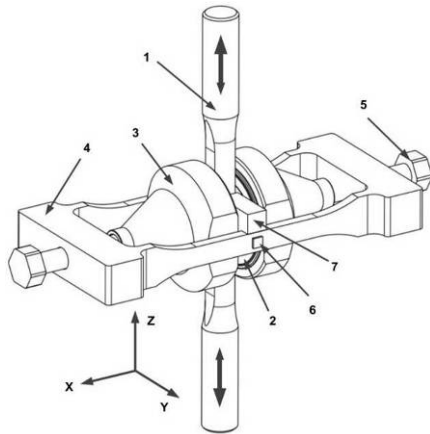


Fig. 53 Figure 1: Penetrant crack indication after removal of the bushing (above) and sectioned cracks (below)



1. Test coupon (Al 7075-T7351)
2. Fretting pads (Steel 17-4PH H1025)
3. Pad rig (Steel)
4. Normal force rig (Steel)
5. Tensioning screw (Steel)

Fig. 54 Fretting fatigue test setup

References

- [1] L. Molent, S.A. Barter and R.J.H. Wanhill, The Lead Crack Fatigue Lifting Framework, DSTO-RR-0353, 2010
- [2] S.A. Barter, L. Molent and R.J.H. Wanhill, Marker Loads for Quantitative Fractography of Fatigue Cracks in Aerospace Alloys, M. Bos (ed.), ICAF 2009, Bridging the Gap between Theory and Operational Practice, 15–54
- [3] F+W Emmen Switzerland, LBF Darmstadt Germany, NLR Amsterdam Netherlands, IABG Ottobrunn Germany, FALSTAFF Fighter Aircraft Loading STAndard For Fatigue, March 1976
- [4] S. Kim, J. T. Burns, R. P. Gangloff, Fatigue crack formation and growth from localized corrosion in Al–Zn–Mg–Cu, *Engineering Fracture Mechanics* 76 (2009) 651–667
- [5] N. Ranganathan et al., Fatigue crack initiation at a notch, *International Journal of Fatigue* 33 (2011) 492–499
- [6] A. Uebersax, C. Huber, G. Renaud, M. Liao, Structural Integrity of a Wing Upper Skin with Exfoliation Corrosion, M. Bos (ed.), ICAF 2009, Bridging the Gap between Theory and Operational Practice, 245–258
- [7] A. Uebersax, C. Huber, I. Kongshavn, A. Gassmann, Fretting Fatigue Testing and Repair Qualification of a Wing to Fuselage Trunnion, ICAF 2013 Proceedings